

Dist: A

ation is estimated to average 1 hour per response, including the time for reviewing instructions, searching existing data sources, completing and reviewing the collection of information. Send comments regarding this burden estimate or any other aspect of this reducing this burden, to Washington Headquarters Services, Directorate for Information Operations and Reports, 1215 Jefferson 12, and to the Office of Management and Budget, Paperwork Reduction Project (0704-0188), Washington, DC 20503.

1. AGENCY USE ONLY (Leave blank)		2. REPORT DATE 12/July/94	3. REPORT TYPE AND DATES COVERED Annual Technical 1/June/93-30/May/94	
4. TITLE AND SUBTITLE Surface Reactivity of Combustion Generated Soot Particles			5. FUNDING NUMBERS PE - 61103D PR - 3484 SA - S1 G - F49620-92-J-0314	
6. AUTHOR(S) Robert J. Santoro			DTIC SELECTED SEP 07 1994 F	
7. PERFORMING ORGANIZATION NAME(S) AND ADDRESS(ES) The Pennsylvania State University Mechanical Engineering/PERC 240 Research Building East University Park, PA 16802				
9. SPONSORING/MONITORING AGENCY NAME(S) AND ADDRESS(ES) AFOSR/NA 110 Duncan Avenue, Suite B115 Bolling AFB, DC 20332-0001			8. PERFORMING ORGANIZATION REPORT NUMBER AFOSR-TR- 94 05161	
11. SUPPLEMENTARY NOTES			10. SPONSORING/MONITORING AGENCY REPORT NUMBER 788 94-29016	
12a. DISTRIBUTION/AVAILABILITY STATEMENT Approved for public release; distribution is unlimited.			12b. DISTRIBUTION CODE A	
13. ABSTRACT (Maximum 200 words) During the second year of this AASERT program, efforts have remained focused on the further development of the laser-induced incandescence technique and the sampling of soot particles from diffusion flames. Characterization of the laser-induced incandescence technique for soot particle measurements in laminar diffusion flames has been completed. In particular, the relationship between laser fluence and the temporal character of the laser-induced incandescence signal has been carefully examined and documented. Based on this work, the technique is currently being extended to soot particle measurements in turbulent diffusion and droplet flames. Concurrently, efforts have continued on developing a sampling system to collect soot particles from laminar diffusion flames. Several modifications to the sampling system have been made to allow for the collection of sample sizes up to 0.1 gm of soot. A heated burner and vaporizer system have also been developed to allow for the study of liquid hydrocarbon fuels. Of particular interest for the present study is the effect of toluene on soot particle surface reactivity. Samples have recently been obtained in a series of laminar diffusion flames and analysis of the samples is currently underway. DTIC QUALITY INSPECTED 3				
14. SUBJECT TERMS Soot particles, surface reactivity, gas turbines, diffusion flames, particle growth			15. NUMBER OF PAGES 77	
17. SECURITY CLASSIFICATION OF REPORT UNCLASSIFIED			16. PRICE CODE	
18. SECURITY CLASSIFICATION OF THIS PAGE UNCLASSIFIED			19. SECURITY CLASSIFICATION OF ABSTRACT UNCLASSIFIED	
20. LIMITATION OF ABSTRACT UL				

Annual Technical Report
on
Surface Reactivity of Combustion Generated Soot Particles

(AFOSR Grant F49620-92-J-0314)

For the Period June 1, 1993 through May 31, 1994

Prepared by

Robert J. Santoro
Department of Mechanical Engineering
The Pennsylvania State University
University Park, PA 16802

Submitted to

Air Force Office of Scientific Research
Bolling Air Force Base
Washington, DC

DTIC QUALITY INSPECTED 3

July 1994

Accession For	
NTIS	CRA&I <input checked="" type="checkbox"/>
DTIC	TAB <input type="checkbox"/>
Unannounced	<input type="checkbox"/>
Justification	
By	
Distribution /	
Availability Codes	
Dist	Avail and/or Special
A-1	

94 9 06 085

Table of Contents

Summary	1
1.0 Introduction	1
2.0 Research Objectives	1
3.0 Research Accomplishments	3
<u>3.1 Sampling of Soot Particles in Laminar Diffusion Flames</u>	3
<u>3.2 Laser-Induced Incandescence Studies</u>	7
4.0 Conclusions	8
5.0 References	9
6.0 Publications	10
7.0 Meetings and Presentations	10
8.0 Participating Personnel	11
9.0 Interactions	11
10.0 Inventions	11

Summary

During the second year of this AASERT program, efforts have remained focused on the further development of the laser-induced incandescence technique and the sampling of soot particles from diffusion flames. Characterization of the laser-induced incandescence technique for soot particle measurements in laminar diffusion flames has been completed. In particular, the relationship between laser fluence and the temporal character of the laser-induced incandescence signal has been carefully examined and documented. Based on this work, the technique is currently being extended to soot particle measurements in turbulent diffusion and droplet flames. Concurrently, efforts have continued on developing a sampling system to collect soot particles from laminar diffusion flames. Several modifications to the sampling system have been made to allow for the collection of sample sizes up to 0.1 gm of soot. A heated burner and vaporizer system have also been developed to allow for the study of liquid hydrocarbon fuels. Of particular interest in the present study is the effect of toluene on soot particle surface reactivity. Samples have recently been obtained in a series of laminar diffusion flames and analysis of the samples is currently underway.

1.0 Introduction

Over the past decade, significant progress has been made in understanding the processes which control the formation, growth and burnout of soot particles in combustion systems. Because the presence of soot particles has significant effects on radiative transfer in gas turbine engines, combustor lifetime is seriously impacted by increases in soot formation as new engine technologies are developed. Consequently, AFOSR has had a continuing effort in the study of soot particle formation aimed at understanding the fundamental processes which control its formation, growth and burnout. This program has emphasized *in situ* diagnostics to study the chemical and physical mechanisms important in the formation and oxidation processes associated with soot particles in combustion systems. These studies have led to one of the most extensive data bases available on the effects of fuel structure, species concentration, operating pressure, residence time and temperature on the processes which control soot formation. The present effort is complementing that program by adding a study aimed at investigating the surface reactivity of the soot particles as a function of these same parameters. An additional objective has emerged recently which deals with the development of a novel laser-based diagnostic technique for measuring soot particle size and concentration. This technique, which is based on laser heating effects to detect and characterize soot particles, is termed laser-induced incandescence. Progress on the characterization of this technique will be reviewed in this report.

The material which follows summarizes the progress made during the second year of this Augmentation Award for Science and Engineering Research Training (AASERT).

2.0 Research Objectives

The soot formation process in combustion systems can be broadly described as: (1) a

precursor chemistry stage in which the large chemical species which lead to the first particles are formed; (2) an inception stage in which a large number of small particles are formed; (3) a surface growth and coagulation stage in which most of the mass is added and particle size increases dramatically; and finally (4) an oxidation stage in which particle burnout can occur. In the present research effort, it is the second stage which is of particular interest.

Recent studies¹⁻⁴ of the surface growth process for soot particles have come to a series of differing conclusions. Although it is generally believed that acetylene (C_2H_2) is the predominant surface growth species in terms of mass addition, the specific mechanism responsible for the surface reactions is not known. Conversely, there is some evidence to indicate that possibly large polynuclear aromatic hydrogen species (PAH) can also have a significant effect.⁵ The current controversy centers on the role that the particle surface area has in the growth mechanism. Some experiments observe a direct dependence on particle surface area,³ while others show little or no dependence.⁴ Furthermore, in all combustion systems, as the soot particles age in the high temperature environment, they are observed to decrease in surface reactivity. Recent papers attempting to resolve this situation have focused on the concept of active sites^{1,2} on the particle surface. It is then the number of these sites which controls the growth rate. As reactions occur at the active sites, they are removed and must be regenerated.² Thus, the loss of surface reactivity would be a result of a decrease in the regeneration mechanism. Some success has been achieved using this approach,^{1,2} but there is no direct measurement support for the details of this mechanism.

Based on the above brief review of the current controversy regarding soot particle surface growth, the present study is aimed at directly measuring the variation in the particle surface reactivity in laminar diffusion flames. In this study, soot particles will be extracted from the flames and analyzed to determine the relative state of the particle surface properties. Conditions are carefully selected to correspond to previous well measured laminar diffusion flames studied in our laboratory. In fact, a series of ethylene flames which have been most extensively characterized⁶ is being studied first. The initial measurements will emphasize soot mass yield, electron spin resonance (ESR) and total surface area (BET) as a function of axial position in the flame. The ESR measurements will yield information on the chemical radical activity of the soot particles⁷ which we argue is related to the number of surface active sites. The BET surface area measurements will yield additional information on the manner in which the surface area available for reaction is changing. These measurements can be used to compare with optical light scattering measurements of this same quantity obtained for these flames in previous studies,⁶ as well as for comparison with recent aggregate interpretations of that data.⁸

Because of the importance of optical techniques for the *in situ* measurement of soot particle properties, current efforts have also emphasized the development of a novel diagnostic, laser-induced incandescence (LII). This technique is based on earlier work by Melton⁹, Dasch¹⁰, Ecbreth^{11,12}, Dec et al.¹³, and Tait and Greenhalgh.¹⁴ The present studies have focused on quantitative *in situ* measurements of soot particle properties. The objective of this work is to establish the measurement capabilities for this technique in a wide variety of steady and unsteady combustion environments.

3.0 Research Accomplishments

3.1 Sampling of Soot Particles in Laminar Diffusion Flames

The work initially reported in our previous annual report has continued during the past year. The work we reported for the first year of the AASERT award in this area summarized the initial efforts of Mr. Matthew Schneider, an undergraduate research student, between the period June 1, 1993 though August 1, 1993. Mr. Schneider developed a sampling system to extract soot particle samples from laminar diffusion flames. A copy of Mr. Schneider's research report is included as Attachment A.

The significant results of his research include the following:

- 1) A sampling system capable of extracting soot from laminar diffusion flames burning ethene and air was developed and tested.
- 2) This sampling approach was proven to be reproducible and robust for the flame conditions examined.
- 3) Comparisons with optical measurements of the soot mass showed systematic differences between the two approaches, but revealed that the general behavior of the soot mass profiles were similar.
- 4) It was recommended to continue development of this system.

As recommended, the sampling system developed by Mr. Schneider has been refined. The basic design for this system involves a burner, a flame quench system, a dilution probe and collection system. The current system is briefly described below. Further details can be found in Attachment A.

Burner System

The burner is a Burke-Schumann type burner consisting of two concentric tubes, with fuel in the center and coflowing air in the annular region (See Figure 1). The burner housing was machined from 2 inch diameter brass. The fuel tube used in this study was 1/2 inch outer diameter with a wall thickness of 0.032 inches. The fuel tube was cut to a length of 20 inches and was made to be movable, or adjustable up and down, through the burner housing. The adjustable nature of the fuel tube was necessary to allow different heights in the flame to be studied.

Flame Quenching System

Initial work on the soot collection system lead to the observation that a screen placed at an axial cross section of a laminar diffusion flame would quench the flame at that particular

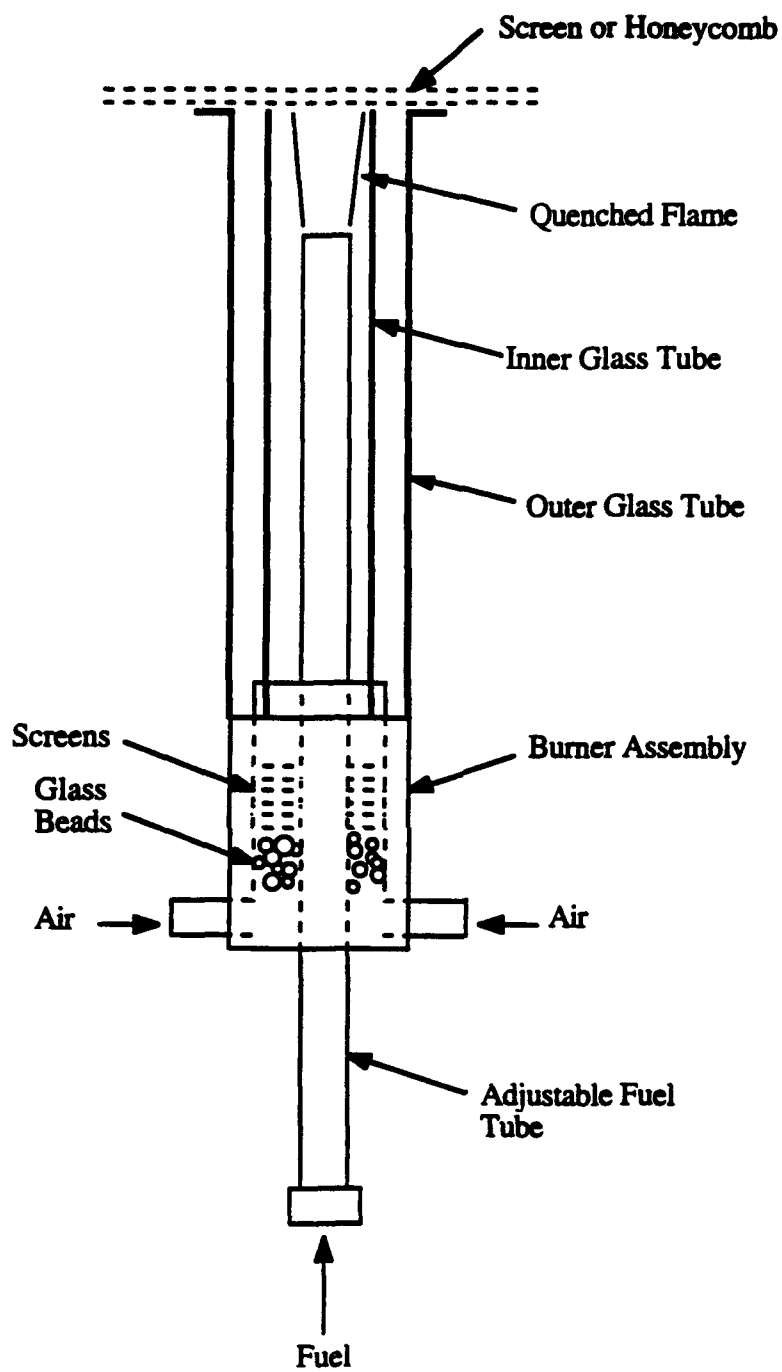


Figure 1: Burner and Flame Quenching Assembly

height. Above the screen, soot particles could be seen emitting from the quenched flame, which occurred without visually disturbing or varying the conditions of the flame below the screen. It was decided that this type of quenching method should be used for the soot collection system. The screen used in these experiments was made from type 304 stainless steel with a wire diameter of 0.017 inches and a mesh size of 0.044 inches.

Figure 1 shows a general description of how the flame quenching occurs. The fuel tube was adjusted so that the height desired to be studied in the flame was measured from the tip of the fuel tube to the top of the inner glass tube (which was aligned with the top of the outer glass tube). To quench the flame, the screen was placed on the flange of the outer glass tube. It was found that if the screen was left sitting over the flame for too long, the screen would become very hot at the quenching location, and soot would plug the cells. To avoid these problems, it was decided to slowly move the screen back and forth during the experiments. This procedure kept the soot from collecting on, and plugging one particular part of the screen.

Dilution Probe Design

The design of the dilution probe allowed for a combination of dilution, collection, and heat exchanger type cooling of the soot (See Figure 2). The probe was made of two concentric brass tubes with inner diameters of 3/8 and 1/2 inches respectively. The inner tube was connected to a filter holder and vacuum line which allowed soot and gases to be drawn into the probe. The two tubes were held in place by a brass fixture near the top of the probe along with a small ring cap at the entrance of the probe. The brass fixture allowed nitrogen to flow through the outer tube and down the probe, producing the heat exchanger effect on the soot and gases entering the probe. The nitrogen was also allowed to enter the vacuum flow of the inner tube through four small (1/16") holes in the inner tube near the bottom of the probe. The nitrogen entering the flow here would serve the purpose of diluting the particles and reactant gases, further cooling of the soot particles. The entire length of the probe was 24 inches to allow sufficient cooling of the soot and gases before entering the filter holder.

Vacuum and Collection System

The vacuum and collection system consisted of a 47 mm Belman Filter Holder, 3 meters of 3/8 inch copper tubing, a Magnehelic pressure gauge (0-100 inches H₂O), a critical orifice to control the flow rate, and a vacuum pump (See Figure 2).

The pressure gauge was used to read the pressure drop across the filter (from atmospheric pressure) which was an indication of the amount of soot collected on the filter. The 3 meters of copper tubing allowed for the gases in the vacuum line to cool to ambient conditions at the critical orifice. The vacuum pump operated at 1/10 of ambient pressure assuring a choked flow through the orifice and a constant mass flow rate through the vacuum line.

Two types of filters have been used in collecting the soot in this project. Both filters were 47 mm diameter Pallflex Teflon Coated Glass Fiber Filters. The filters used for most of

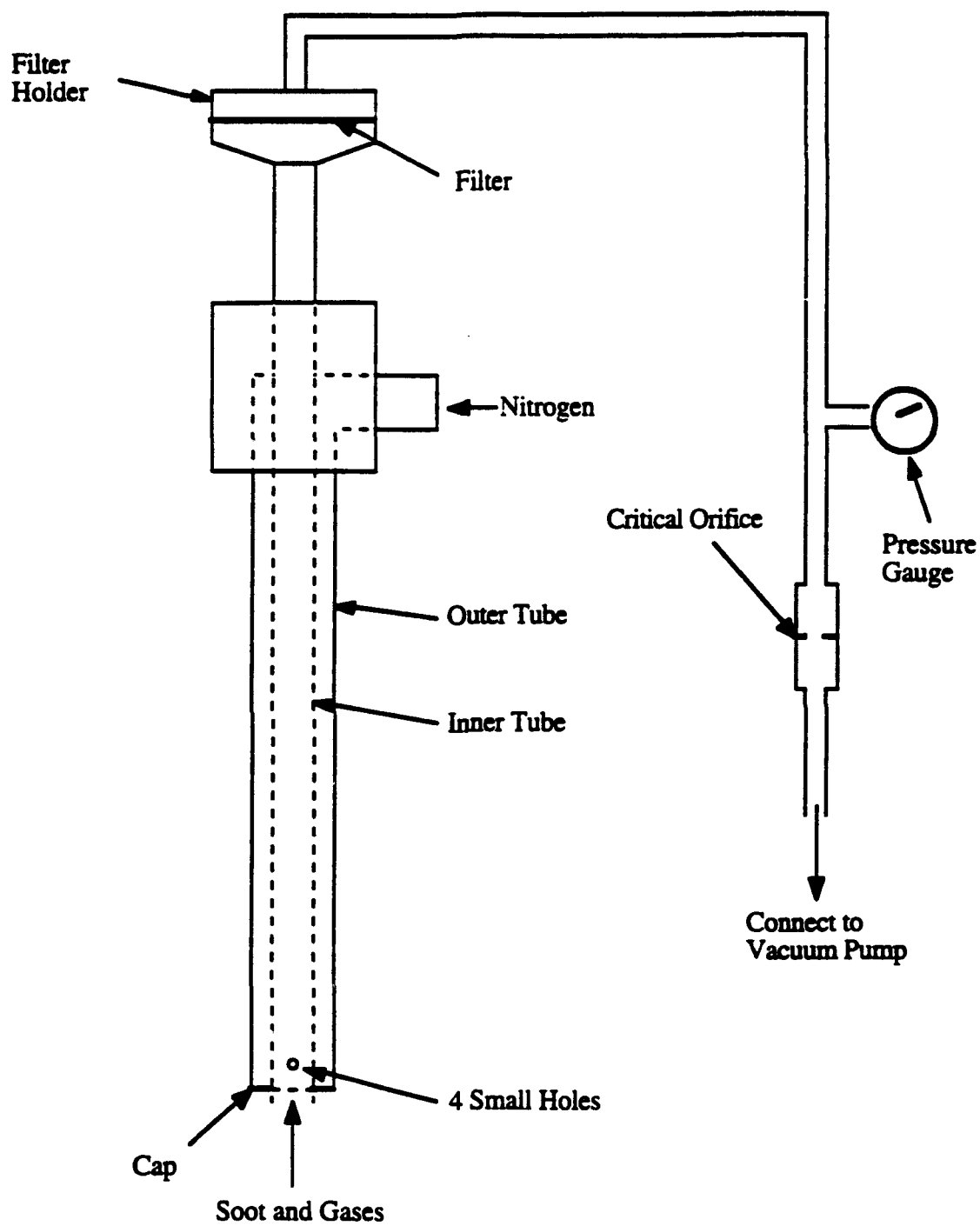


Figure 2: Dilution Probe and Collection System

the experiments were type T60A20 and have a reported collection efficiency of 70 to 80% for 0.035 μm particles and at least 95% for particles with diameters of 0.3 μm and larger. The other filters used in some of the experiments were type TX40HI20 and had a reported collection efficiency of 98 to 99% for 0.035 μm particles and 99 to 100% efficiency for particles with diameters of 0.3 μm and larger.

The above described system has been modified to include a rotating screen to assist in reducing blockage by soot particle deposition. Additionally, a new burner has been assembled which is similar to the burner used in previous studies.^{6,8} This burner also has provisions to heat the incoming air and fuel which allows the study of temperature effects as well as the use of liquid fuels. Tests involving liquid fuels also require a vaporizer to introduce the fuel. An appropriate vaporizer system has been developed and tested.

Technical problems in producing steady, well behaved flames using this heated burner have required a substantial time commitment during the past year. These problems are now solved and soot samples are currently being acquired. Samples as large as 0.1 gm have been collected and are now being analyzed in terms of available surface area as a function of flame conditions.

Current efforts are focused on collecting and analyzing soot samples in a variety of flames as well as increasing the collection capacity of the sampling system to large sample sizes on the order of 1 gm. Larger quantities of soot are desirable to allow repeated measurements as well as the application of several analysis approaches.

3.2 Laser-Induced Incandescence Studies

The studies of laser-induced incandescence (LII) have focused on soot measurements in laminar diffusion flames. The results of these studies have recently appeared in an article published in *Combustion and Flame* which is included as Attachment B.

Based on this study, the following conclusions concerning the LII diagnostic of soot volume fraction are made:

- (1) Laser-induced incandescence has been used to obtain spatially-resolved measurements of soot volume fraction in laminar diffusion flames, in which comparisons with laser scattering/extinction data yield excellent agreement for both radial profiles and integrated volume fraction. Thus, laser-induced incandescence can be used as an instantaneous, spatially-resolved diagnostic of soot volume fraction without the need for the conventional line-of-sight laser extinction method.
- (2) The temporal characteristics of the laser-induced incandescence signal is observed to involve a rapid rise in intensity followed by a relatively long (ca. 600 ns) decay period subsequent to the laser pulse, while the effect of laser fluence is manifest

in non-linear and saturated response of the laser-induced incandescence signal with the transition occurring at a laser fluence of approximately $1.2 \times 10^8 \text{ W/cm}^2$ for laser pulse of ca. 7 ns in duration.

- (3) Spectral response of the laser-induced incandescence involves a continuous spectrum in the visible wavelength range due to the blackbody nature of the emission, where the spectral response for 300-450 nm wavelength range indicates a soot surface temperature of ca. 5000 K with the spectrum continuing at a nearly level intensity up to 750 nm wavelength due to the multiplicity of the soot particle sizes in the probe volume.
- (4) Simultaneous measurements of LII and the vertically-polarized light-scattering yield encouraging results concerning the mean soot particle diameter and number concentration; thus significant applications exist in two-dimensional imaging and simultaneous measurements of laser-induced incandescence and light-scattering to generate a complete soot property characterization.

4.0 Conclusions

During the second year of the current AASERT grant, "Surface Reactivity of Combustion Generated Soot Particles" the following results have been achieved:

- 1) A sampling system for the extraction of soot particles from laminar diffusion flames has been developed and tested.
- 2) A new burner system has been developed which incorporates a vaporizer and heated flow system to allow studies of temperature effects and liquid fuels species on soot surface reactivity.
- 3) The current sampling techniques have been demonstrated to be capable of collecting quantities up to 0.1 gm and efforts are underway to extend that to 1 gm quantities.
- 4) The LII technique has been demonstrated to be capable of quantitative soot volume fraction measurements in laminar diffusion flames. These results have been published.
- 5) LII measurements are currently being extended to turbulent diffusion and droplet flames.

During the second year of the AASERT award Mr. Bryan Quay, a graduate student in Mechanical Engineering, has been supported under the grant. Mr. Quay has worked on both the soot sampling and LII experiments. Mr Matthew Schneider assisted Mr. Quay as part of an NSF summer research program. Recently, Mr. Chris Chandler has joined the project under

support from Lubrizol, an oil and fuels additive company. Mr. Chandler's research is complementary to the AASERT objectives and illustrates the dual-use aspects of the research.

5.0 References

1. Woods, I. T. and Haynes, B. S., "Soot Surface Growth at Active Sites," *Combustion and Flame*, 85, pp. 523-525 (1991).
2. Frenklach, M. and Wang, H., "Detailed Modeling of Soot Particle Nucleation and Growth," *Twenty-Third Symposium (International) on Combustion*, The Combustion Institute, Pittsburgh, PA, pp. 575-582 (1990).
3. Harris, S. J. and Weiner, A. M., "Surface Growth of Soot Particles in Premixed Ethylene Air Flames," *Combustion Science and Technology*, 31, pp. 155-167 (1983).
4. Wieschowsky, U., Bookhorn, H. and Fetting, F., "Some Observations Concerning the Mass Growth of Soot in Premixed Hydrocarbon-Oxygen Flames," *Twenty-Second Symposium (International) on Combustion*, The Combustion Institute, Pittsburgh, PA, pp. 343-352 (1988).
5. Howard, J. B., "Carbon Addition and Oxidation Reactions in Heterogeneous Combustion and Soot Formation," *Twenty-Third Symposium (International) on Combustion*, The Combustion Institute, Pittsburgh, PA, pp. 1107-1127 (1990).
6. Santoro, R. J., Yeh, T. T., Horvath, J. J. and Semerjian, H. G., "The Transport and Growth of Soot Particles in Laminar Diffusion Flames," *Combustion Science and Technology*, 53, p. 89 (1987).
7. Wagner, H. Gg., "Soot Formation in Combustion," *Seventeenth Symposium (International) on Combustion*, The Combustion Institute, Pittsburgh, PA, pp. 3-19 (1979).
8. Dobbins, R. A., Santoro, R. J. and Semerjian, H. G., "Analysis of Light Scattering From Soot Using Optical Cross Sections for Aggregates," *Twenty-Third Symposium (International) on Combustion*, The Combustion Institute, Pittsburgh, PA, pp. 267-275 (1988).
9. Melton, L. A., "Soot Diagnostics Based on Laser Heating," *Appl. Opt.*, 23, pp. 2201-2208 (1984).
10. Dasch, C. J., "Continuous-Wave Probe Laser Investigation of Laser Vaporization of Small Soot Particles in a Flame," *Appl. Opt.*, 23, pp. 2209-2215 (1984).

11. Eckbreth, A. C., Bonczyk, P. A. and Verdick, J. F., *Prog. Energy Combust. Sci.*, 5:253-322 (1979).
12. Eckbreth, A. C., *Appl. Physics*, 48:4473-4479 (1977).
13. Dec, J. E., zur Loye, A. O. and Siebers, S. L., *SAE TEchnical Papers Series SAE-910224*, Society of Automotive Engineers, PA (1991).
14. Tait, N. P. and Greenhalgh, D. A., "2D Soot Field Measurements by Laser Induced Incandescence," *Proceedings of the "Optical Methods and Data Processing In Heat Transfer and Fluid Flow" Conference*, London, April 1992.

6.0 Publications

Quay, B., Lee T-W, Ni, T. and Santoro, R. J., "Spatially-Resolved Measurements of Soot Volume Fraction Using Laser-Induced Incandescence," *Combustion and Flame*, 97:384-392 (1994).

7.0 Meetings and Presentations

"Soot Formation Workshop," AFOSR Contractors Meeting on Air Breathing Combustion, Atlantic City, NJ, June 14, 1993.

"Measurements of Soot Growth Species Concentration In Diffusion Flames," 1993 Technical Meeting of the Eastern States Section of the Combustion Institute, Princeton University, Princeton, NJ, October 25-27, 1994.

"New Techniques for Quantitative, Planar Soot Measurements," 1993 Technical Meeting of the Eastern States Section of the Combustion Institute, Princeton University, Princeton, NJ, October 25-27, 1994.

"Spatially-Resolved Measurements of Soot Volume Fraction Using Laser-Induced Incandescence," 1993 Technical Meeting of the Eastern States Section of the Combustion Institute, Princeton University, Princeton, NJ, October 25-27, 1994.

"Modeling and Measurements of Soot and Species in a Laminar Diffusion Flame," The 1994 Western States Section Meeting of the Combustion Institute, University of California/Davis, Davis, CA, March 21-22, 1994.

8.0 Participating Personnel

Dr. Robert J. Santoro, Professor of Mechanical Engineering
Mr. Bryan Quay, Graduate Student, Department of Mechanical Engineering
(Ph.D. expected July, 1995)
Mr. Chris Chandler, Graduate Student, Department of Mechanical Engineering
(M.S. expected June, 1995), supported by Lubrizol - 1994-1995
Mr. Gregory Davis, Undergraduate Student, Department of Electrical Engineering
Ms. Vicki Jacobs, Undergraduate Student, Work Study Lab Assistant
Mr. Matthew Schneider, Undergraduate Student, supported under the NSF
Undergraduate Summer Research Program in Mechanical Engineering - 1993
Mr. Jed Bailey, Undergraduate Student, supported under the NSF Undergraduate
Summer Research Program in Mechanical Engineering - 1994
Mr. Daniel Boone, Technician, Department of Mechanical Engineering

9.0 Interactions

Lubrizol, Wickeliffe, OH - Drs. Ralph Kornbrekke and Dan Daly

A project under the support of Lubrizol was initiated as of January, 1994 to undertake a collaborative research program to examine the surface reactivity of soot particles which are formed under conditions of interest to Diesel engine combustion. The objective of this research is provide appropriate characterization of the soot particle surface to allow development of appropriate additives which would suppress the deleterious effects of soot particles on engine lubricants.

10.0 Inventions

No inventions have resulted during the second year of this program.

Attachment A

Design of a Soot Sampling System for Laminar Diffusion Flames

Penn State Summer Undergraduate Research Program:

**Design of a Soot Sampling System for
Laminar Diffusion Flames.**

Submitted by:

**Matthew A. Schneider
Department of Mechanical Engineering
The University of Iowa
Iowa City, IA 52240**

Submitted to:

**Dr. R.J. Santoro
Department of Mechanical Engineering
Penn State University
University Park, PA 16802**

Submitted on:

July 30, 1993

ABSTRACT

Recent studies have disagreed about the role that particle surface area plays in the surface growth of soot particles. The concept of active sites on the particle surface has been suggested to solve this controversy. This concept is promising, but, there have not been any direct measurements of the number of radical active sites on soot particles to support this theory. The objective of this project was to design and test a soot sampling system capable of sampling soot from different heights in laminar diffusion flames for the purpose of these studies. Before these studies can be performed, the capability of the soot sampling system to obtain particles representative of the particles in the flame has to be assessed.

The soot sampling system studied in this project consisted of a flame quenching system utilizing either a screen or a metal honeycomb. The soot was subsequently diluted and collected through the use of a dilution probe connected to a filter holder vacuum pump. The experiments in this project were used to determine the capability of the designed soot collection system.

The results of the experiments performed showed that the soot sampling system was capable of collecting soot samples from the flame, and creating reproducible results for the percent conversion of fuel to soot calculated from these samples. The dilution probe, utilizing Nitrogen as a dilution gas, was also found to be effective because it was found to decrease the temperatures of the soot and gases being collected on filters.

Flame profiles of percent conversion of fuel to soot were found using the soot collection system, and compared to laser scattering results. The soot collection results showed the same trends and peaks as the laser scattering results. However, the soot collection results were much higher than the laser scattering results for low flame heights sampled, but, then dropped below the laser scattering results higher in the flame. Experiments were performed to determine if the reasons for these trends could be found. The results from the experiments did not solve the problem with the disagreement in the data, but provide a useful starting point for further development of the soot collection design.

ACKNOWLEDGEMENTS

The first people I would like to acknowledge in this report, are the people who made this experience and working on this project possible. I would first like to thank the Department of Mechanical Engineering at Penn State University for giving me the opportunity to take part in the summer undergraduate research program at this institution. I would also like to thank the National Science Foundation for funding and supporting programs like this across the country which make it possible for undergraduate engineering students to perform useful research projects and maintain an interest in higher academic pursuits in engineering.

The second people I would like to acknowledge, are the people who assisted me in working on the research project this summer. I would first like to extend a thanks to my advisor, Dr. R.J. Santoro, for the initial project idea, and all of the input to the direction of the project and advice as the project progressed. I would also like to thank all of the students I came into contact with this summer that lent me a helping hand when I was trying to find my way around a new environment. I would especially like to thank Darrel Rapp and Simon Leonard for their inciteful ideas and education on the concepts and equipment associated with this project. Without them I would probably still be sitting at my desk trying to figure out exactly how to attack this project. I would also like to thank Daniel Boone for his construction of the experimental apparatus used in this project.

The last people I would like to thank are my professors at The University of Iowa for their support, and especially Professor L.D. Chen, for sparking my interest in the field of combustion (no pun intended) and his support of my academic career as a Mechanical Engineering student.

TABLE OF CONTENTS

	Page
INTRODUCTION.....	1
EXPERIMENTAL.....	2
RESULTS AND DISCUSSION.....	9
CONCLUSIONS AND RECOMMENDATIONS.....	21
APPENDICES.....	25
Appendix A: Proposed Experiments and Initial Work.....	25
Appendix B: Rotameter Calibration.....	29
Appendix C: Tabled Data.....	44
Appendix D: Lubrizol Study Summary.....	46
REFERENCES.....	49

INTRODUCTION

Soot is what gives many flames their yellow color due to its blackbody emission. But, soot is a common, and typically undesirable, by-product of many combustion processes. The detrimental effects of soot range from unwanted emissions from engines and smokestacks, to decreased engine efficiency and lifetime due to soot's high radiative heat transfer properties (McKinnon, 1979). Understanding the fundamental processes which control the formation, growth, and burnout of soot is essential for reducing combustion emissions and continuing new engine technologies.

Soot is a solid material primarily composed of carbon, and is formed in flame conditions. The formation process of soot in combustion can be broken down into four main steps. The first step is a chemistry stage in which fuel pyrolysis creates polycyclic aromatic hydrocarbons (PAH's) which, in turn, form very small spherical particles (Frenklach and Wang, 1990). The second stage is an inception stage in which the number of small particles forming is drastically increased (Santoro, 1993). Particle size and mass increase dramatically as these particles undergo surface growth and coagulation in the third stage. And, last, the particles experience an oxidation stage in which the particles can either burnout or be emitted from the flame (Santoro, 1993).

A considerable number of flame studies, utilizing both intrusive and non-intrusive methods, have led to a vast amount of knowledge into the processes which underlie the formation of soot in combustion. However, recent studies investigating the surface growth stage of soot formation have led to differing conclusions on the factors effecting this particular process. A general belief is held that acetylene is the major species of mass addition in the surface growth of soot. However, the exact mechanism responsible for the surface growth reactions with acetylene is not known, and there have been differing theories for the role particle surface area plays in these reactions. Some studies have concluded that increased growth rate of soot (controlled by an increased equivalence ratio in flames) is due to increased surface area available for growth, and is not dependent on the concentration of the surface growth species (Harris and Weiner, 1982). While later studies have questioned these conclusions and shown little dependence of the particle surface growth on surface area (Wieschnowsky, 1989).

It is known that as soot particles age in flames, their surface reactivity is observed to decrease (Santoro, 1993). Current papers attempting to resolve the controversy involving the role of surface area, have proposed that the surface growth mechanism is dependent on the number of available active sites on the particle surface, and not dependent on the total surface area available for reactions (Frenklach and Wang, 1990, and Woods and Haynes, 1991). Frenklach and Wang (1990) have developed a kinetic model for the growth of PAH's by reactions with acetylene. In this model, larger PAH's are formed by the addition of acetylene to radical active sites on the surface of smaller PAH's, and growth continues due to a self-regeneration of the radical sites in the reactions. Woods and Haynes (1991) have proposed that soot growth occurs under the same mechanisms. They believe that soot grows through reactions of growth species with surface active sites, and a subsequent regeneration of the sites. They have calculated soot radical site densities from their model and shown that they decrease logarithmically with the age of the particles. This agrees with the knowledge that surface reactivity of soot particles decreases with age, and dispels the direct dependence of surface growth on the surface area of the particle. However, there have not been any direct measurements of the number of radical active sites on soot particles to support the details of this mechanism.

It has been proposed by Santoro (1993) to attempt to measure directly the particle surface reactivity variation of soot in laminar diffusion flames. In order to do this, soot

particles must be extracted from the flame and then analyzed. Initial measurements would focus on electron spin resonance (ESR) and total surface area (BET) of soot particles as a function of axial position in the flame. ESR would give information on the chemical radical activity of soot particles, and it is argued that this would directly relate to the number of active sites on the surface of the particle. Additional information on the available surface area for reactions would be obtained using the BET surface area measurements.

A diffusion flame is a flame in which the mixing rate of the fuel and oxidizer is slow compared to their reaction rate. In these flames, the fuel and oxidizer come together through molecular and turbulent diffusion and form a reaction zone (Glassman, 1987). The burning rate of a diffusion flame is controlled by the rate at which the fuel and oxidizer are brought together (Glassman, 1987). This control of the flame conditions and ease of varying these conditions is one of the main reasons why diffusion flames are useful to study. The laminar diffusion flame is perhaps the most basic flame and its conditions can be easily reproduced. The particular flame proposed for the initial study of the surface reactivity of soot particles would be an ethylene/air diffusion flame (Santoro, 1993). The reason for studying this flame is due to the large amount of information on soot concentration, species concentration, and velocity and temperature profiles obtained from previous studies (Santoro, 1987). These previous studies can be used to assess the results of the surface reactivity measurements and identify other capabilities associated with these studies.

In order to perform the soot surface reactivity studies, a method for obtaining soot samples from the flames has to be developed. The initial soot sampling system must have the capability of collecting soot at different axial flame cross sections. The soot samples from these collections will then represent average values for soot surface reactivity and surface area for the particular height in the flame (Santoro, 1993). The soot sampling system must also have the capability of immediately diluting the soot with an inert gas after it is removed from the flame, in order to cool the soot and prevent further reactions of the particles with reactant gases (Santoro, 1993). Before soot samples are collected for the surface reactivity measurements, this soot collection system must be designed and tested to ensure that the soot samples are representative of the soot particles at the particular flame height (or, to ensure that the soot collection system is functioning properly). The objective of this project was to accomplish this task, and design, construct, and test a soot sampling system which could be used for the soot surface reactivity studies.

Initially, three different methods were proposed for collecting soot from the laminar diffusion flames. Each of these methods involved a flame quenching system (a method for cutting off the flame, or stopping the flame reactions at a particular height), a particle dilution system, and a collection (or vacuum) system. The details of these proposed methods and the initial work with these methods are outlined in Appendix A. The results from the initial work refocused the ideas for the proposed soot collection systems, and this paper concentrates on the particular design decided upon, and the results of tests performed associated with this design.

EXPERIMENTAL

The soot collection system design used for these experiments can be broken down into primarily four parts: a burner system, a flame quenching method, a particle dilution and collection probe, and a vacuum system.

Burner System

The burner used in this study was a Burke-Schumann type burner consisting of two concentric tubes, with fuel in the center and coflowing air in the annular region (See Figure 1) (Burke, 1928). The burner system was used in previous experiments (Leonard, 1993) and only a few modifications were made to the system. The burner housing was machined from 2 inch diameter brass. The fuel tube used in this study was 1/2 inch outer diameter, 0.032 inch thick half hard brass. The fuel tube was cut to a length of 20 inches and was made to be movable, or adjustable up and down, through the burner housing. The adjustable nature of the fuel tube was necessary to allow different heights in the flame to be studied (this will be described shortly).

Air entered the base of the annular region through two ports and flowed through an approximately 1 inch layer of 3mm diameter beads, and then through six layers of 70 gauge screen to ensure a laminar flow of air. An 11 inch long inner glass tube with an outer diameter of 1.26 inches and an inner diameter of 1.14 inches, was fitted inside the burner housing with a strip of teflon tape near the bottom, to ensure a good seal to the housing. This tube was used to constrain the air flow and ensure a stable flame. An 11 inch long outer glass tube with an inner diameter of 2 inches was fitted over the outside of the burner housing, concentric to the inner glass tube. The outer glass tube had a flange at its top and was used primarily to hold the flame quenching system of the soot collection system (See Figure 1).

Fuel and air were supplied to the burner assembly through pressurized cylinders, and the flow was monitored using Matheson Gas Glass Tube Rotameters. The rotameters were calibrated using soap film bubble flow meters and a description of the calibration procedure and results can be found in Appendix B.

Flame Quenching System

Initial work on proposed designs for the soot collection system lead to the knowledge that a screen placed at an axial cross section of a laminar diffusion flame would quench the flame, or cut it off, at that particular height. Above the screen, soot particles could be seen emitting from the quenched flame, and the quenching of the flame would take place without visually disturbing or varying the conditions of the flame below the screen. It was decided that this type of quenching method should be used for the soot collection system. Another method that was decided to be attempted for quenching the flame, was to use a metal honeycomb, as was performed for obtaining CO concentrations at flame heights by Roper *et. al.* (1977).

The screen used in these experiments was made from type 304 stainless steel with a wire diameter of 0.017 inches and a mesh size of 0.044 inches. The screen was used to quench the flame for the majority of experiments performed in this paper. A piece of honeycomb was also used for some of the tests. Initially, three different cell sizes of honeycomb were tested, 1/32 inch, 1/16 inch, and 1/8 inch. It was found that the 1/32 and 1/16 inch cell sizes would expand part of the flame just below the honeycomb (below the quench) considerably. Because these honeycombs altered the flame conditions, they could not be used for experiments. The honeycomb used for the experiments in this paper was manufactured by Kentucky Metals, had a cell size of 1/8 inch and was made of 0.004 inch Hastelloy® X Foil. The height of the honeycomb was 0.275 inches.

Figure 1 shows a general description of how the flame quenching took place for this project. The fuel tube was adjusted so that the height desired to be studied in the flame

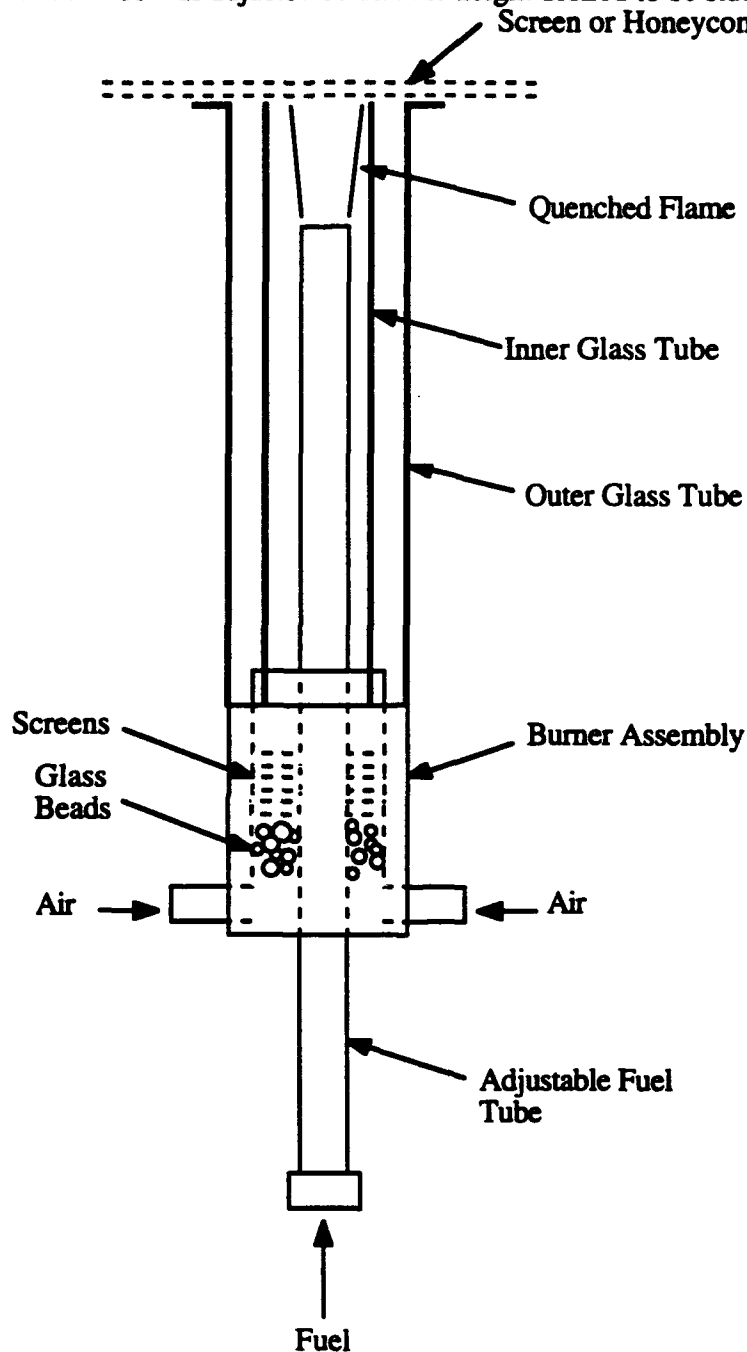


Figure 1: Burner and Flame Quenching Assembly

was measured from the tip of the fuel tube to the top of the inner glass tube (which was aligned with the top of the outer glass tube). For this project, these heights were measured with a small metal ruler. The flame was then ignited and allowed to stabilize. To quench the flame, the screen or honeycomb was placed on the flange of the outer glass tube. It was found that if the screen was left sitting over the flame for too long, the screen would begin to get very hot at the quenching location, and soot would begin to plug the cells. To

avoid these problems, it was decided to slowly move the screen (or honeycomb) back and forth during the experiments. This kept the soot from collecting on , and plugging one particular part of the screen. A screen moving system consisting of a translating laser table stand was designed to simplify and make consistent the moving of the screen, however, the parts for this system were never completed. This will be discussed later in the Conclusions and Recommendations section of this report.

Dilution Probe Design

The dilution probe design decided upon, was a modification of the dilution probe described in Appendix A. The design of the dilution probe allowed for a combination of dilution, collection, and heat exchanger type cooling of the soot (See Figure 2).

The probe was made of two concentric brass tubes with inner diameters of 3/8 and 1/2 inches respectively. The inner tube was connected to a filter holder and vacuum line which allowed soot and gases to be drawn into the probe. The two tubes were held in place by a brass fixture near the top of the probe and by a small ring cap at the entrance of the probe. The brass fixture allowed Nitrogen to be pumped through the outer tube and flow down the probe, producing the heat exchanger effect on the soot and gases entering the probe. The Nitrogen was also allowed to enter the vacuum flow of the inner tube through four small (1/16") holes in the inner tube near the bottom of the probe. The Nitrogen entering the flow here would serve the purpose of diluting the particles from reactant gases, and further cooling of the soot particles. The entire length of the probe was 24 inches to allow sufficient cooling of the soot and gases before entering the filter holder.

Nitrogen flow entering the dilution probe was controlled by a Matheson Gas Glass Tube Rotameter which was calibrated using a dry gas meter (See Appendix B).

For many of the experiments, the temperature of the soot and gases leaving the probe and entering the filter holder was measured using a K-type sheathed and grounded thermocouple. This thermocouple was inserted into the flow through the probe by the use of Swagelock® fittings at the top of the probe.

Vacuum and Collection System

The vacuum and collection system was identical to the system used by Leonard *et al.* (1993). It consisted of a 47 mm Belman Filter Holder, 3 meters of 3/8 inch copper tubing, a Magnehelic pressure gauge (0-100 inches H₂O), a critical orifice to control the flow rate, and a vacuum pump (See Figure 2).

The pressure gauge was used to read the pressure drop across the filter (from atmospheric pressure) which was an indication of the amount of soot collected on the filter. The 3 meters of copper tubing allowed for the gases in the vacuum line to cool to ambient conditions at the critical orifice. The vacuum pump operated at 1/10 of ambient pressure assuring a choked flow through the orifice and a constant mass flow rate through the vacuum line (Leonard, 1993).

The vacuum line flow was calibrated using a dry test meter, and the nominal flow rate through a clean filter was found to be 157 cc/s (9.4 L/min). This translates to a velocity of gases through the probe of 220 cm/s. It was also found that the flow through the vacuum line could be found by using the dilution probe, and the Nitrogen flow through the probe. To perform this, the end of the dilution probe was plugged while the vacuum pump was running. The Nitrogen flow was then adjusted until the pressure gauge read a

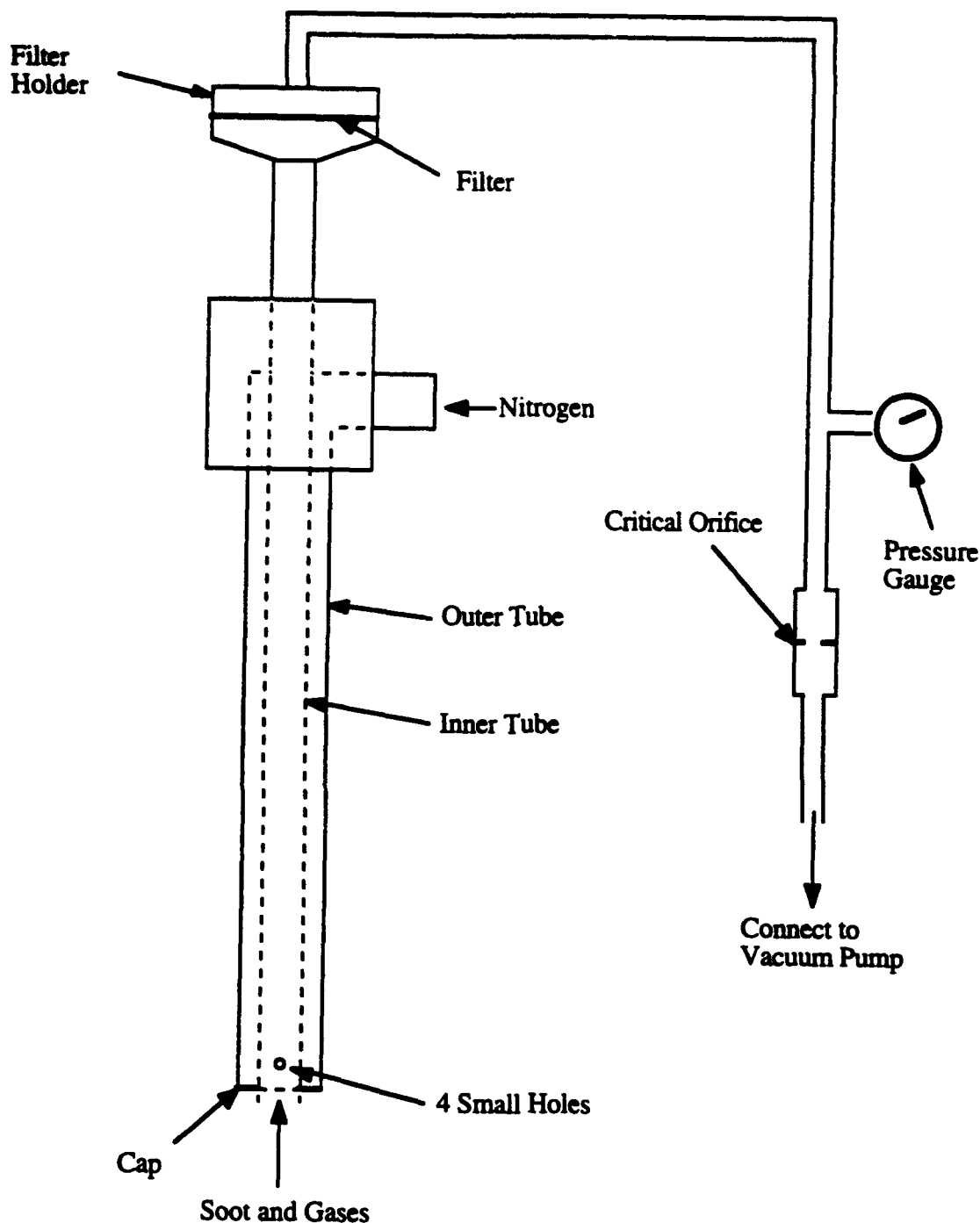


Figure 2: Dilution Probe and Collection System

constant value (the value before plugging the end of the probe). The vacuum line flow could now be read flow in the Nitrogen flow meter. This procedure was performed to study the effects of filter pressure drops (from collected soot) on the characteristics of the vacuum line flow. The flow was studied for pressure drops ranging from 0 to 60 in of H_2O , and the results are seen in Table 1 and Figure 3. The results show that the vacuum line flow seems to decrease at an almost constant rate no matter what the pressure drop across the filter. It is believed that this decrease in flow is not due to unchoking the critical

orifice, but, as the pressure drop across the filter increases, the pressure behind the critical orifice decreases changing the flow conditions through the entire vacuum line. It is believed that the flow remains choked, but because of this pressures decrease, the choked mass flow rate decreases (Zucrow, 1976). This was important to know, because it could have an effect on how the results of experiments were interpreted.

Table 1: Filter Pressure Drop Effects on Vacuum Line Flow

Pressure Drop in H ₂ O	Vacuum Flow cc/s	% Change from Initial
0	165	0.00
2	165	0.00
9	16	2.42
12	158	4.24
21	156	5.45
25	153	7.27
30	150	9.09
35	148	10.30
40	146	11.52
45	144	12.73
50	142	13.94
56	140	15.15
60	138	16.36

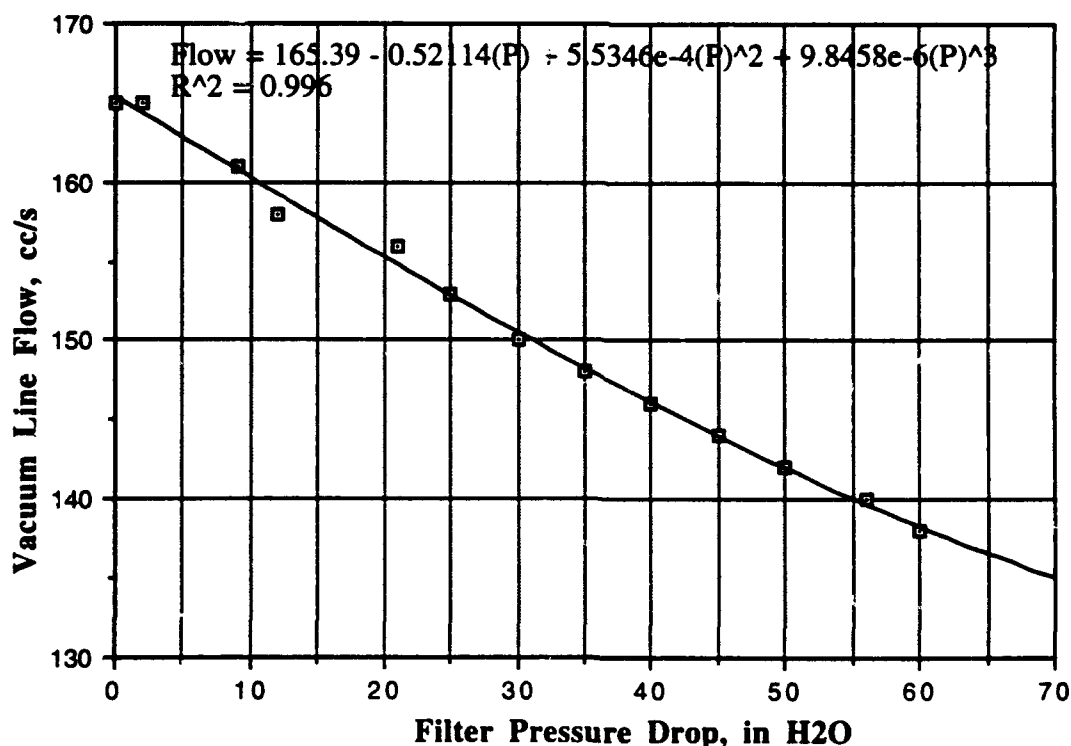


Figure 3: Vacuum Line Flow as a Function of Filter Pressure Drop

There were two types of filters used in collecting the soot in this project. Both filters were 47 mm diameter Pallflex Teflon Coated Glass Fiber Filters. The filters used for most of the experiments were type T60A20 and have a reported collection efficiency of 70 to 80% for 0.035 μm particles and at least 95% for particles with diameters of 0.3 μm and larger (Liu, 1983). The other filters used in some of the experiments were type TX40HI20 and had a reported collection efficiency of 98 to 99% for 0.035 μm particles and 99 to 100% efficiency for particles with diameters of 0.3 μm and larger (Liu, 1983).

Flame Conditions

As was mentioned, it was proposed to study ethylene/air diffusion flames to assess the initial capabilities of the soot collection system. The flame used for most of the studies in this project was an overventilated ethylene/air laminar diffusion flame with a fuel flow of 3.85 cc/s. This flame has an approximate flame height of 82 mm and does not emit any soot. Another flame used in this project was a 4.90 cc/s overventilated ethylene flame. This flame is a sooting flame and emits a fair amount of soot. For this reason, this flame does not have a measurable flame height. The flame conditions used in this project are outlined in Table 2.

Table 2: Experimental Flame Conditions

Flame	Fuel	Fuel Flow cc/s	Fuel Velocity cm/s	Air Flow cc/s	Air Velocity cm/s
Flame 1	Ethylene	3.85	4.00	233.3	34.4
Flame 2	Ethylene	4.90	5.09	233.3	34.4

Experimental Procedure

The purpose of the experiments performed in this paper were to study the concepts of the soot collection design, to determine the reliability of results that could be obtained with this design, and to study the effects of different experimental factors on the collection of the soot.

The main method behind these experiments was to first adjust the height of the burner tube to correspond to the height of the flame desired to study. A filter was weighed (mg) with a Metler AE100 scale (accurate to 0.0001 g) and placed in the filter holder. The flame was ignited and allowed to stabilize. When the flame was stable, the screen (or honeycomb) was placed on the holder, and the dilution probe (with vacuum on and a set Nitrogen flow rate) was moved directly over the cut-off flame at a height of approximately 3 mm above the screen. The screen was slowly moved to keep it from clogging, and soot was collected until the pressure gauge read about 25-30 inches of H_2O pressure drop across the filter. At this point, the probe was removed. Each collection time was recorded with a stop watch, and the mass of the soot was measured by weighing the filter again after collection. Another parameter recorded for some of the experiments was the temperature of the gases entering the soot trap. When temperatures were recorded, the temperature before collection and just before removing the probe from above the flame were noted.

With the mass of the soot collected and the time of collection recorded, the mass flow rate of soot (g/s) was calculated using Equation 1. The mass flow rate of the fuel

$$\dot{m}_s = \frac{m_s}{t} \quad \text{Eq. 1}$$

was found by first determining its room temperature density from the ideal gas equation (Eq. 2). With the properties of the fuel, this density was found to be 0.2279 kg/m^3 . The mass flow rate could then be calculated by multiplying the fuel density times the volumetric flow rate (Q_f) (Eq. 3). The two flow rates of fuel and soot could now be used to calculate a

$$\rho = \frac{P}{R T} \quad \text{Eq. 2}$$

$$\dot{m}_f = \rho Q_f \quad \text{Eq. 3}$$

percent conversion of fuel to soot by simply dividing the two (Eq. 4). This method,

$$\% \text{ Conversion} = \frac{\dot{m}_s}{\dot{m}_f} 100 \quad \text{Eq. 4}$$

however, does not take into account that the probe may not be capturing all of the soot emitted from the quenched flame, especially under high Nitrogen dilution flows (the Nitrogen dilution effects the efficiency of the probe to collect soot). A different factor, the smoke yield (ϵ_s), was used by Leonard *et. al.* (1993) under a slightly different method for collecting soot from flames. The smoke yield was calculated by multiplying the quotient of the mass flow rates times a dilution factor (f_{dil}) (Eq. 5). The dilution factor was found by dividing the total flow rate of all the gases in the system (F_T) by the flow rate through the probe (f_p) (Eq. 6).

$$\epsilon_s = \frac{\dot{m}_s}{\dot{m}_f} f_{dil} \quad \text{Eq. 5}$$

$$f_{dil} = \frac{F_T}{f_p} \quad \text{Eq. 6}$$

The smoke yield was calculated for many of the experiments performed in this project, although the exact application of the equation for this soot collection system was questioned. It was decided that a modification of the equation may work better for this system, and this will be discussed later.

RESULTS AND DISCUSSION

The experiments performed with this soot collection system, were used to determine if the system was functioning correctly, and would give reproducible results. Another motive behind these experiments was to determine how Nitrogen dilution through the probe would affect the experimental conditions and results. Unless otherwise mentioned, for all of these experiments, Flame 1 was used in conjunction with a screen quench and the type T60A20 filters.

For the first experiments, only one flame height was studied, and several soot samples were collected to determine the reproducibility of the results for soot collection. The height at which the flame was quenched for this study was 41 mm, which was approximately half of the 3.85 cc/s flame height. Initially, the Nitrogen flow through the

dilution probe was set to zero, and several soot collections were performed. During collection, the probe seemed to capture all of the soot rising above the screen and did so without any large observable effects on the flame below the screen. However, as the screen was moved, the flame would move slightly, and there was also an observed effect that if the probe was not directly over the quenched flame, the flame would pull slightly toward the probe. The percent conversion values (Eq. 4) along with the smoke yield (Eq. 5) were calculated, and the results for these collections are seen in Table 3.

Table 3: Soot Collection Results, Height = 41mm, N₂ Flow = 0 cc/s

Soot Mass Flow *10 ⁻⁴ (g/s)	% Conversion Fuel To Soot	Smoke Yield
1.77	20.18	0.305
1.59	18.13	0.274
1.97	22.46	0.340
2.17	24.74	0.374
1.92	21.89	0.331
	Average = 21.48	Average = 0.325
	$\sigma = 2.48$	$\sigma = 0.038$

As can be seen from Table 3, the results were fairly reproducible with some variation between each sample. However, these were the first samples taken with the system, and the exact method for taking the samples had not yet been practised or perfected, probably causing some variation in the data. It was decided that these results could serve as a base condition for studying the effects of Nitrogen dilution on the soot collection.

The next experiment performed was the same as the first, except in this experiment, the Nitrogen flow* through the probe was set to 66.67 cc/s (4 lpm), and soot was collected several times. Under these conditions, the Nitrogen did not show any effect on the flame below the screen, and may actually have helped to counteract the tendency of the flame to be drawn toward the probe when not perfectly aligned. However, with Nitrogen being introduced into the probe, some of the soot was escaping and not being captured in the probe. The results for these collections can be seen in Table 4.

In order to further test the effects of Nitrogen dilution on the base conditions, for the next collection, the Nitrogen flow was set to 100 cc/s (6 lpm). With these conditions, a considerable amount of soot escaped the probe at times. Also, the Nitrogen flow would sometimes disturb the flame below the screen and cause it to flicker and become slightly unstable. The results for these collections can be seen in Table 5. In order to further test the Nitrogen effects on the flame, one more test was performed with the Nitrogen flow at 133.3 cc/s (8 lpm). Under these conditions, when the probe was placed over the quenched flame, the flame would become completely unstable, and the Nitrogen would actually cause some additional unstable quenching of the flame.

* It should be mentioned that the rotameter used for these initial Nitrogen flows was a Matheson Gas #605 rotameter, which was rather inaccurate for the small flows used. For later experiments, a #604 rotameter was used which allowed setting the Nitrogen flows more accurately.

Table 4: Soot Collection Results, Height = 41mm, N₂ Flow = 66.7 cc/s

Soot Mass Flow *10 ⁻⁴ (g/s)	% Conversion Fuel To Soot	Smoke Yield
1.57	17.90	0.347
1.75	19.95	0.387
1.98	22.58	0.437
1.79	20.41	0.395
Average = 20.21		Average = 0.392
$\sigma = 1.92$		$\sigma = 0.037$

Table 5: Soot Collection Results, Height = 41mm, N₂ Flow = 100 cc/s

Soot Mass Flow *10 ⁻⁴ (g/s)	% Conversion Fuel To Soot	Smoke Yield
1.35	15.39	0.331
1.62	18.47	0.397
1.62	18.47	0.397
1.75	19.95	0.429
Average = 18.07		Average = 0.389
$\sigma = 1.92$		$\sigma = 0.041$

When comparing the results of the three tables, it can be seen that the percent conversion of soot (Eq. 4) decreased slightly as the Nitrogen dilution was increased. This was expected due to the fact that as the Nitrogen flow was increased, some of the soot would escape the probe and not be collected. The smoke yield calculated (Eq. 5) for these results can also be seen to vary without any noticeable trend for the three cases. If the experiments were performed correctly, and if equation 5 held for these experiments, the results for the smoke yield should have been almost identical for each case. It is believed that most of the reason why these results are not identical is because the smoke yield used by Leonard *et. al.* (1993) does not hold for these experiments. It was not clear how the smoke yield equation should have been modified, but later experiments will discuss attempts at discovering how this should be accomplished.

Now that the capability of the soot collection system to collect soot and give fairly reproducible results had been assessed, it was decided to discover the characteristics of soot sampled from different heights in the flame. In order to study these characteristics, profiles of the flame were made by collecting soot at certain intervals of flame height. Since a method for weighting the results from Nitrogen dilution (smoke yield) had not been discovered, the Nitrogen dilution was set to zero for these flame profiles. Both Flame 1 and Flame 2 were profiled, and tabled results can be seen in Tables C1 and C2, respectively, in Appendix C.

Since Flame 1 and 2 differed in flame height, it was necessary to calculate a non-dimensional height parameter to compare the results from the two flames. The height parameter (η) used, was the same as calculated for experiments by Santoro *et. al.* (1987) (Eq. 7). In equation 7, z is the height (cm), D is a diffusion coefficient ($0.156 \text{ cm}^2/\text{s}$ for

$$\eta = \frac{z D}{V} \ln \left(1 + \frac{1}{S} \right) \quad \text{Eq. 7}$$

ethylene), V is the fuel flow rate (cc/s), and S is the ratio of volume of air to volume of fuel required for complete combustion (14.28 for ethylene) (Santoro, 1987).

The flame profile data was very important, because it could be compared to previous data collected on these flames to determine if the soot being collected was actually representative of soot at the heights being studied. In order to examine this, the percent conversion of fuel to soot was plotted against the non-dimensional height parameter for the two flames, along with results for percent conversion obtained through laser scattering by Santoro *et. al.* (1987). These plots can be seen in Figure 4.

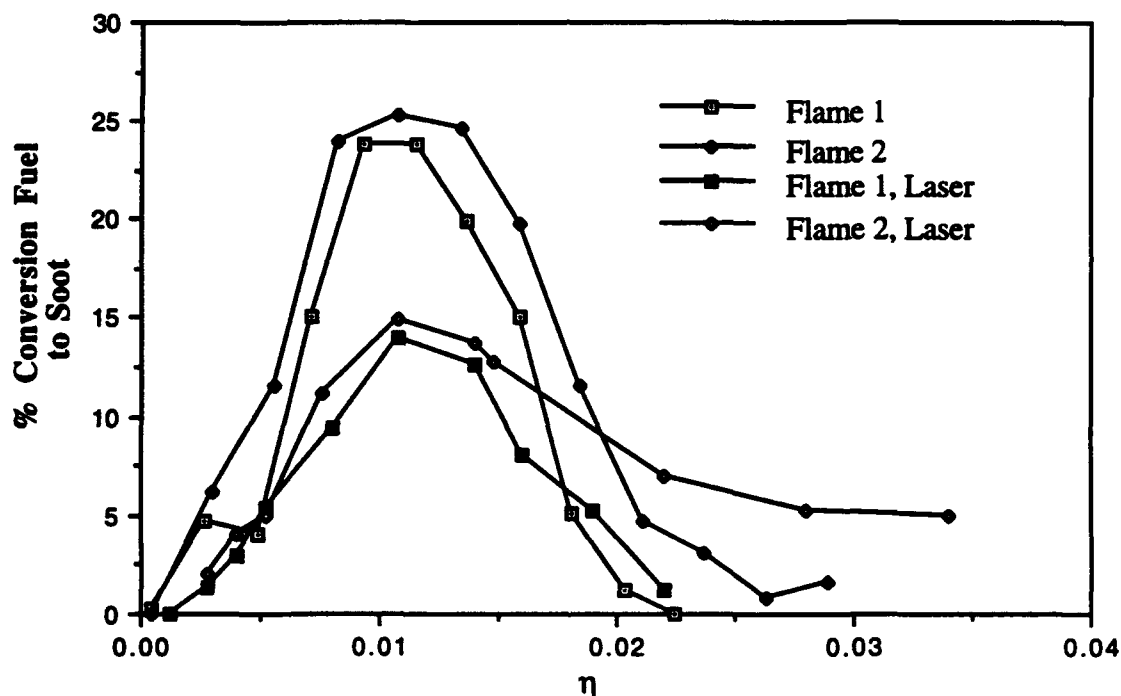


Figure 4: Percent Conversion of Fuel to Soot for Ethylene

The comparison of the results obtained through soot sampling to those obtained from laser scattering show some interesting trends. First, Figure 4 shows that the soot collection results showed the same general trends and the same peak locations as the laser scattering results. However, it can also be seen that the soot sampling results were considerably higher than the laser scattering results for the majority of the flame, until near the top of the flame. At this point, the soot sampling results fell below the laser scattering results. In order to verify that the soot sampling results were correct, and these results were not due to an error in the measurements, another flame profile of Flame 1 was performed and compared to the first flame profile. The data for this flame profile can be found in Table C3 in Appendix C, and the results are plotted in Figure 5.

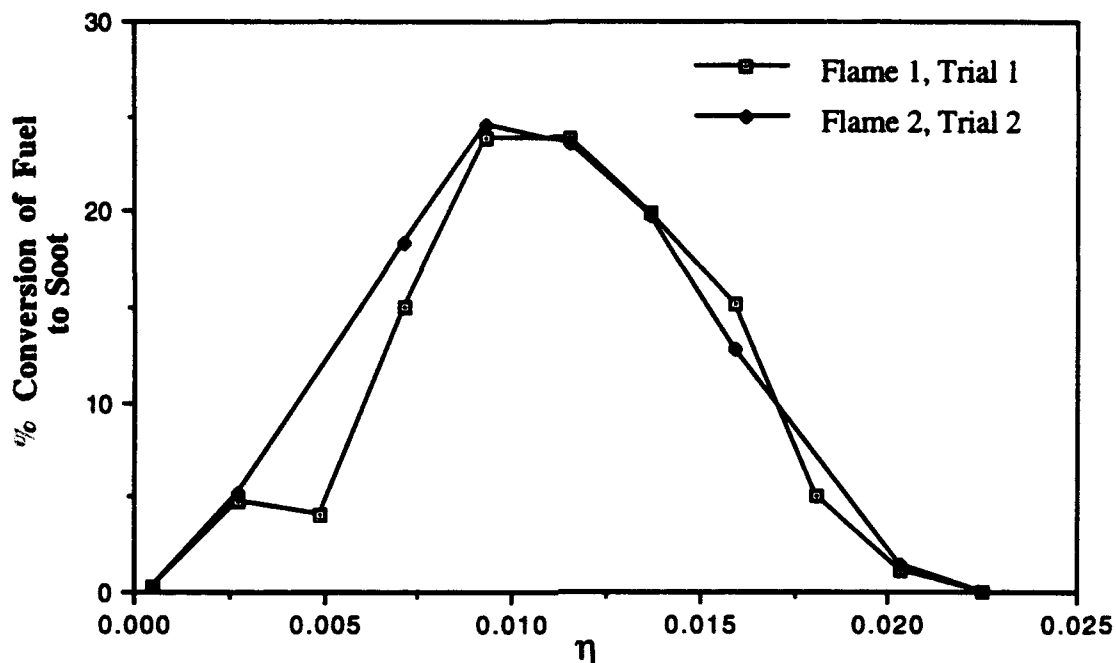


Figure 5: Reproduced Percent Conversion of Fuel to Soot for Ethylene

Figure 5 shows that the flame profile results were almost perfectly reproduced for Flame 1, so it was deduced that there were not errors in the experimental method used for collecting the soot samples. However, these results reinforced the fact that the soot being collected was not agreeing with the results from laser scattering experiments. Many of the experiments performed after this concentrated on discovering why the soot collection system might be having these problems.

It was believed that the collected soot flame profile was generally higher than the laser scattering results because the filters were collecting other things, such as water moisture and polycyclic aromatic hydrocarbons, which are formed in the flames. In order to determine if this was true, it was decided to bake some of the filters after soot had been collected on them, and see if this changed their mass. This procedure and results will be discussed later in the paper. Another reason why the soot collected was showing different results than the laser scattering, could have been due to the fact that the particles were not being diluted before they were collected, allowing the reactions to continue. For this reason, the Nitrogen dilution system was studied in more detail.

Two main factors were of importance in studying the effects of Nitrogen dilution on the soot collection: the soot mass flow rate (percent conversion of fuel to soot), and the temperature of the gases collected with the dilution probe. The effects of the height in the flame and the Nitrogen dilution flow rate on these parameters were studied. For these experiments Flame 1 was used with the screen quenching system. The effect of Nitrogen flow rate on the soot collection had been studied briefly previously (See Tables 3, 4, and 5). However, the effects could not be studied in detail due to the fact that the rotameter being used was too large to measure the Nitrogen flows accurately (#605 Matheson Gas Rotameter). A new #604 rotameter was used for these experiments.

In order to study the temperatures of the gases in the dilution probe, it was desired to mount a thermocouple inside the probe just above the Nitrogen inlet holes. After much deliberation and studying the effects on the thermocouple output if it would accidentally touch the side of the probe, it was decided that this would not be feasible without excessively disrupting the soot collection procedure. So, the thermocouple mounted in the gas flow directly before the soot trap was used. It was decided that the temperatures at this point would demonstrate the ability of the Nitrogen to dilute the particles. However, this configuration would make it difficult to determine exactly what factor was influencing the dilution the most (either conduction and convection to the probe, or the actual mixing of the Nitrogen with the combustion gases).

The first Nitrogen dilution effect studied, was the Nitrogen flow rate through the probe which would first start to disturb the flame below the screen quenching system. The flame was set to be quenched at a height of 66 mm and the dilution probe was placed a few millimeters above the screen. The Nitrogen flow was slowly increased until the flame began to flicker as a result of the flow. The Nitrogen flow was then backed off slightly and this flow was noted. This flow was found to be 98 cc/s. The same test was attempted at a height of 42 mm and the same result was found. A lower height in the flame should have been tested, but was not, and it was later found that even 90 cc/s Nitrogen dilution flow rate would disturb the flame when sampling at heights around 10 mm. Later tests confirmed that the maximum Nitrogen flow rate without disturbing the flame below the screen at this height was 81 cc/s.

Now that a maximum Nitrogen flow had been determined, the Nitrogen flow could be varied from zero to around this value, and the effects on the temperature and soot mass flow could be studied. Due to a low number of filters (at the time) the flame height to be sampled was set at 66 mm. This height allowed for longer collection times, and easier reading of the temperature of thermocouple. Soot was collected for five different Nitrogen flows ranging from 0 to 95 cc/s and the time of collection was kept roughly constant at around 15.5 seconds. For each collection, the temperature before sampling and directly after sampling were noted in order to determine a temperature difference, which was then used to calculate a temperature rate of rise (C/s) (Eq. 8). The temperature rate of rise was

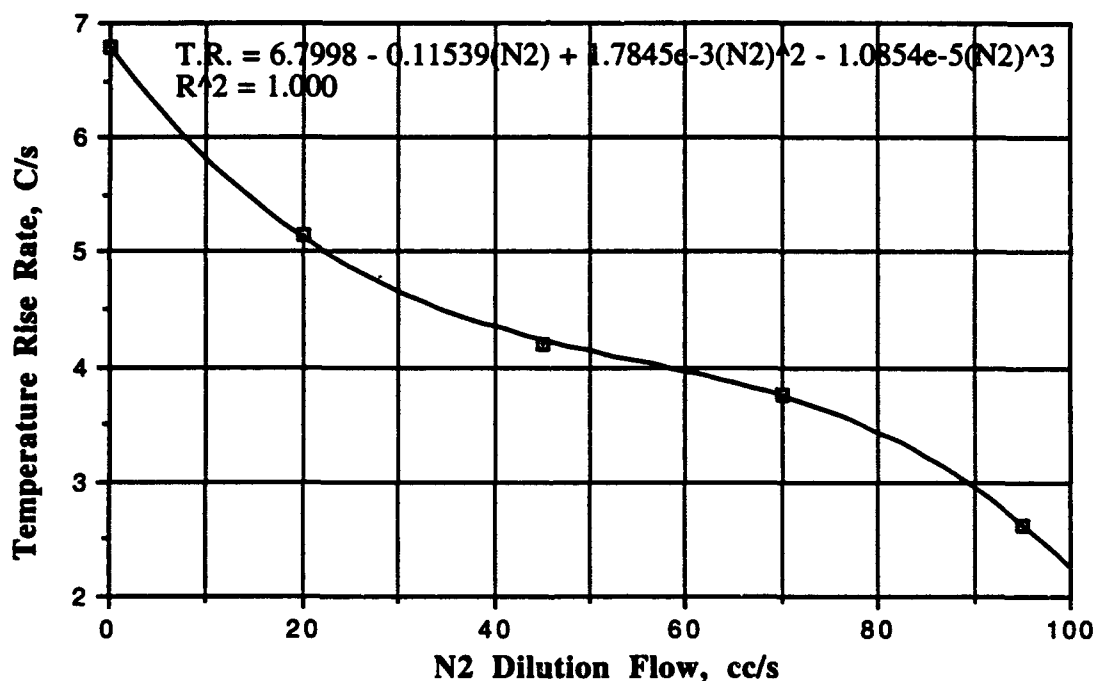
$$\text{Temp. Rise Rate} = \frac{\Delta T}{t} \quad \text{Eq. 8}$$

calculated because it was found that for the sampling times being used, the temperature did not reach a maximum value, but kept increasing. Another height of 42 mm was studied, but only two Nitrogen flow rates were attempted at this height (due to low number of filters). The collection time at this height was kept constant at 8 seconds. The results for all of the runs are seen in Table 6.

From Table 6, it can be seen that the results for the percent conversion of fuel to soot were sporadic, which was not expected. It is not known why these results did not show a particular trend, but it could be due to human errors in running the sampling system. Also, the scale used to find the mass of the soot collected is only accurate to 0.1 mg, and it is questioned if the scale is actually this accurate. Since the soot samples are small (from 0.7 to 2.2 mg, depending on the height), this could lead to large errors in the results. Regardless of this result, it was interesting to note how the temperature rise rate decreased as the Nitrogen dilution increased. To further study this, the temperature rise rate at the 66 mm quench was plotted against the Nitrogen flow and curve fitted with a third order polynomial. This graph is shown in Figure 6.

Table 6: Nitrogen Dilution Study Results

Height mm	N ₂ Dilution cc/s	% Conversion Fuel to Soot	Final Collection Temp. C	Temp. Rise Rate C/s
66	0	3.68	128.2	6.79
66	20	4.41	102.8	5.15
66	45	2.21	88.6	4.19
66	70	2.21	82.2	3.77
66	95	2.94	64.5	2.63
42	0	21.44	81.9	7.33
42	95	19.95	55.6	4.24

**Figure 6: Dilution Effects on Sampling Temperature Rise, Height = 66 mm**

Since it was found that the temperature kept rising during the sampling for these experiments, it was decided to determine if the temperature leveled off and reached a peak, and how long this would take. These experiments were performed the same as previous experiments, except the soot was sampled for as long as it took for the temperature to level off. It was found that for long sampling times, the temperature never did reach a peak, but the temperature rise rate just slowed (similar to an exponential function). It is believed that the temperature keeps rising because the flow rate through the probe decreases as the amount of soot on the filter increases (See Table 1 and Figure 3). Because of the decreased flow through the probe, the amount of air or dilution gas is not being drawn into the probe

as quickly, causing the temperature to increase further. It was also found that if the screen was not moved, the temperature that the soot and gases achieved was higher than if the screen was moved at a fairly high rate. This was interesting to note that the temperature of the soot and gases was effected by the rate at which the screen was moving.

Because of the problems with determining a maximum temperature of the soot and gases entering the filter, it was decided to record the temperature when the filter pressure drop reached approximately 60 in H₂O. These temperatures were recorded for flame heights of 10, 42, and 66 mm, with no Nitrogen dilution and 90 cc/s of Nitrogen dilution. The results can be seen in Table 7, and again, show that the Nitrogen dilution has the effect of cooling the soot and gases entering the filter.

Table 7: Temperature Maximums for 60 in H₂O Pressure Drop

Height mm	Nitrogen Flow cc/s	Maximum Temp. C
10	0	95.0
10	90	63.3
42	0	107.2
42	90	80.2
66	0	122.0
66	90	93.5

Earlier, it was suggested that the smoke yield equation (Eq. 5) could be modified for the dilution probe, to determine soot mass flows when Nitrogen dilution was used. The next step in this project was to determine if such a modification was possible. The factor f_{dil} in this equation was calculated by dividing the total flow rate of all the gases in the system, by the flow rate of the gases through the probe (vacuum line flow). This equation assumes that the flow through the probe is constant due to choking by a critical orifice in the vacuum line. It was already found that the flow in the vacuum line decreases as soot collects on the filter. So, it would be difficult to obtain a completely accurate calculated smoke yield (or dilution factor) that would reflect the soot mass flow rate.

In order to further study what effect the Nitrogen dilution has on the collection of soot, an ideal dilution factor value was calculated using the data from Table 6. Ideally, when the Nitrogen flow is zero, the dilution factor should equal one. As the Nitrogen dilution increases, the dilution factor should also increase to account for the soot that will not be drawn into the probe because of the extra Nitrogen flow. Using the data from Table 6, an ideal dilution factor value was calculated by dividing the percent conversion of soot value for no Nitrogen flow by the percent conversion of soot value measured for the corresponding Nitrogen flow (Eq. 9). These results should show that if a dilution factor

$$f_{dil, ideal} = \frac{\% \text{ Conv. } N_2 = 0 \text{ cc/s}}{\% \text{ Conv. } N_2} \quad \text{Eq. 9}$$

can be found to describe the probe effects, the ideal dilution factor value at different heights for the same Nitrogen flow rate, should be about the same. Table 8 shows these calculations, and also shows that the ideal dilution factor value for the Nitrogen flow of 95 cc/s at 42 mm and 66 mm is considerably different. This also adds to the doubt that the

exact factors effecting the efficiency of the probe to collect soot, and thus, a dilution factor equation can be found for the probe.

Table 8: Ideal Dilution Factor Values for Different Nitrogen Flows

Height mm	N ₂ Dilution cc/s	% Conversion Fuel to Soot	ϵ_s	f_{dil} (ideal)
66	0	3.68	3.68	1
66	20	4.41	3.68	0.834
66	45	2.21	3.68	1.665
66	70	2.21	3.68	1.665
66	95	2.94	3.68	1.252
42	0	21.44	21.44	1
42	95	19.95	21.44	1.075

As was mentioned earlier, it was believed that the percent conversion of fuel to soot values from the soot collection were higher than laser scattering results because of the possibility of the filter collecting moisture and PAH's. The next experiment performed was a combination of studying the effects of using different types of filters, and baking the filters, on the measured percent conversion of fuel to soot. For this experiment, both the T60A20 filters (used in all previous experiments), and TX40HI20 filters (higher efficiency than the T60A20) were used.

In the experiment, soot was collected for three different heights in Flame 1 of 10, 42, and 66 mm respectively. At each of these heights, each type of filter was used to collect soot when there was not any Nitrogen dilution. Then, again, each type of filter was used to collect soot for a Nitrogen dilution of 90 cc/s. All of the filters were baked, including a clean one of each type of the filters as a control, to see if the filters would change mass due to degradation. The filters were weighed before and after soot collection, after one hour of baking at 200 C, and again after another hour of baking at 200 C (total of two hours). The effects of the baking and the filter type could then be studied from the calculated percent conversions of fuel to soot.

The results from this experiment can be seen in Tables 9 and 10 (Table 9 for no Nitrogen dilution, Table 10 for 90 cc/s Nitrogen dilution). It should be noted that at the flame height of 10 mm, the Nitrogen dilution of 90 cc/s was found to seriously disturb the flame below the screen quenching system and could have effected the results at this point. Also, it should be noted that the control filters both did not change mass at all until after the last hour of baking, at this time, their measured mass was found to have decreased by 0.1 mg.

Table 9: Results of Baking Filters, N₂ Flow = 0 cc/s

Filter Type	Height mm	η	% Conv. 1*	% Conv. 2**	% Conv. 3***
T60A20	10	0.0027	5.37	5.10	5.10
T60A20	42	0.0115	22.78	22.78	22.78
T60A20	66	0.0181	3.45	3.95	3.45
TX40HI20	10	0.0027	5.23	5.23	4.83
TX40HI20	42	0.0115	23.04	24.32	23.04
TX40HI20	66	0.0181	5.86	6.60	5.86

* 1 is % Conversion before baking

** 2 is % Conversion after 1 hr bake at 200 C

*** 3 is % Conversion after 2 hr bake at 200 C

Table 10: Results of Baking Filters, N₂ Flow = 90 cc/s

Filter Type	Height mm	η	% Conv. 1*	% Conv. 2**	% Conv. 3***
T60A20	10	0.0027	4.00	3.76	3.53
T60A20	42	0.0115	20.15	20.15	20.15
T60A20	66	0.0181	4.09	3.72	3.34
TX40HI20	10	0.0027	4.32	4.04	4.04
TX40HI20	42	0.0115	18.73	17.63	16.53
TX40HI20	66	0.0181	3.67	3.14	2.62

* 1 is % Conversion before baking

** 2 is % Conversion after 1 hr bake at 200 C

*** 3 is % Conversion after 2 hr bake at 200 C

The results in these tables show that there were not any marked effects of baking the filters on changing the percent conversion of fuel to soot. The values did change in some cases and showed probably the most drastic changes during the last hour of baking. It was mentioned, however, that the control filters had decreased in mass by an amount that was similar to the change in mass of the other filters. This could possibly mean that the filters were beginning to degrade, but, due to the precision and possible accuracy problems with the scale being used to measure the mass of the filters, it is hard to determine whether filter degradation or scale problems were causing the changes.

When looking at Tables 9 and 10, it can also be seen that the effect of the filter type used showed very sporadic results. For the Nitrogen dilution of zero, in some cases, the TX40HI20 filters showed a higher efficiency while in other cases were about the same as the T60A20 filters. However, for the Nitrogen dilution of 90 cc/s, the TX40HI20 filters showed about the same or lower values as the T60A20. These results were actually somewhat disturbing because there were not any trends showing a higher collection

efficiency for the TX40HI20 filters. The variation in the results must have come about from errors induced in the experiment and collection of the soot.

Another factor that was recorded in this experiment was the temperature of the gases entering the soot trap (sometimes not very accurately though). Again a temperature rise rate was calculated for each case, and these results showed some interesting trends (that were expected) and are shown in Table 11. Almost all of the temperature rise rates were seen to decrease as Nitrogen dilution was increased, except for the very low height in the flame (in which problems were incurred anyway). And, it was found that the highest temperature rise rates were occurring for sampling sections in the middle of the flame height. This is due to the fact that there is a large amount of soot in this part of the flame, and the soot is the main heat transfer mechanism in the flame.

Table 11: Soot Collection Temperature Results from Filter Baking Experiment

Height mm	N ₂ Dilution cc/s	Peak Temp. C	Temp. Rise Rate C/s
10	0	47.8	0.58
10	0	71.5	1.3
10	90	67.0	1.7
10	90	68.0	1.5
42	0	76.1	5.32
42	0	78.5	5.95
42	90	58.7	2.67
42	90	55.0	2.85
66	0	100.4	3.24
66	0	100.2	4.80
66	90	73.8	1.60
66	90	72.3	2.15

The last experiments performed in this project involved using the honeycomb to quench the flame. First, the temperatures reached for a 60 in H₂O filter pressure drop were found for heights of 10, 42, and 66 mm. These temperatures were found without using any Nitrogen dilution, just to compare to the temperatures obtained using the screen to quench the flame (Table 7). The results are summarized in Table 12, and show that the honeycomb and screen quenching methods give approximately the same temperatures at the entrance to the filter holder. However, when sampling, it was noticed that the honeycomb would get considerably warmer (or conduct more heat) than the screen had.

**Table 12: Screen and Honeycomb Temperature Results,
Pressure Drop = 60 in of H₂O, N₂ Flow = 0 cc/s**

Quenching Device	Height mm	Maximum Temp. C
Screen	10	95.0
Honeycomb	10	97.2
Screen	42	107.2
Honeycomb	42	101.3
Screen	66	122.0
Honeycomb	66	122.0

Since the temperature results were approximately the same for the two quenching methods, it was desired to determine if the soot collection results would be the same. To determine this, a flame profile of Flame 1 was performed using the honeycomb quenching method. The honeycomb quench worked well except for heights low in the flame. At these points, the suction from the probe would sometimes affect the flame below the honeycomb quench. The data for the flame profile can be found in Table C4 in Appendix C. A plot was made of the results along with the Trial 1 and Trial 2 of the screen quenching method. The laser scattering results (Santoro, 1987) are also shown (Figure 7).

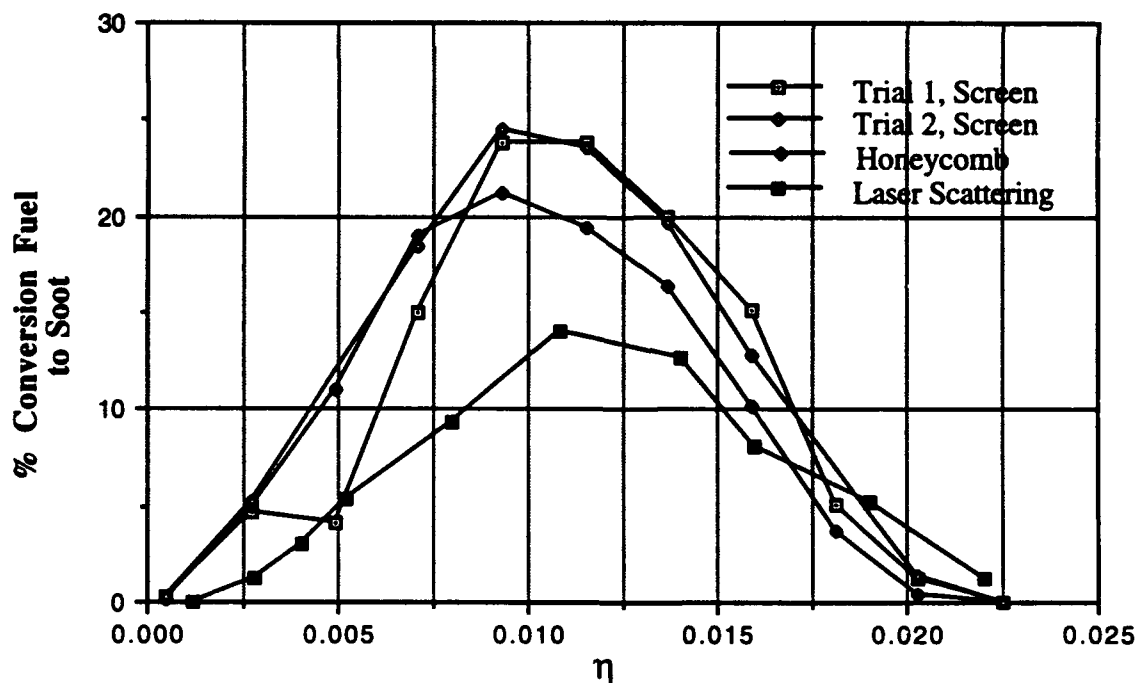


Figure 7: Flame Profiles of Flame 1 from Different Quenching Methods

The results from the honeycomb quench show interesting trends when compared to the screen and laser scattering results. It can be seen that in about the lower 1/3 of the

flame, the honeycomb and screen results are almost the same, but for the remainder of the flame, the honeycomb results are much lower than those from the screen quench. Also, the honeycomb results were still higher than the laser scattering results, until near the top of the flame where they were lower (and even lower than the screen quenching results). It is not sure why the results for the honeycomb showed the trends that they did, but, it is obvious that the honeycomb was having a different quenching effect on the flame than the screen was.

CONCLUSIONS AND RECOMMENDATIONS

The objective of this project was to design a soot sampling system that was capable of sampling soot from different heights in coannular laminar diffusion flames. The system was also to have the capability of diluting the soot particles as they were sampled so they would retain the properties from the location they were removed in the flame. The soot sampling system designed and tested in this project consisted of a flame quench utilizing a screen or honeycomb, and a subsequent collection of the soot emitted from the quench with a dilution probe. The tests and experiments described in this paper were performed to ascertain whether the soot collection system was working, and to study if the soot being collected was representative of the soot in the flame. The general findings were that the system is useful for collecting soot and giving reproducible results, but needs to be studied further to determine if the soot being collected would be useful for experiments such as ESR and BET.

An extensive number of experiments performed with this soot collection system were described in this paper. Perhaps the most important results describing the usefulness of the system came from the comparison of laser scattering results to flame profiles of percent conversion of fuel to soot obtained with the system. Initially, results using a screen quench showed the same general trends and peaks as the laser scattering results. However, the soot collection system showed higher values than the laser scattering results for about the lower 2/3 of the flame. Above this point, the soot collection results dropped below the laser scattering results. It was proposed that this was due to PAH's, present in the flame at lower heights, collecting on the filters. Baking the filters at 200 C for two hours showed that this did not drastically effect the mass of the soot on the filters. This could be due to the fact that the PAH's on the filters were larger, and thus had a higher boiling point than 200 C. Experiments could be attempted in which the filters are baked at a higher temperature to test this hypothesis, but the temperature limits on the filters before they begin to degrade, may limit this type of a test. Another solution to this problem would be to develop some other method for separating (or measuring) the carbon content of the materials collected on the filters.

Although the possibility of large PAH's collecting on the filter could be the answer to why the soot collection results were higher than the laser scattering results, there could be other possibilities. When the flame was quenched with the honeycomb, the flame profile obtained showed the same trends as the screen quench, but with lower values. This could point to a systematic error in the soot sampling system. Because the soot particles exiting the quenched flame were not immediately diluted to stop reactions, the trends in the flame profiles may be describing continued reactions of the particles before they are collected. In the lower portion of the flame, soot collection results showed higher results than laser scattering. This could be due to the fact that the particles (after quenching, and before collection) were continuing growth reactions above the quenching zone. And, higher in the flame, where oxidation and burnout occur, the particles may have been continuing these reactions before collection. This type of analysis describes the trends of the flame profiles obtained with the soot collection system, and may describe why the honeycomb and screen showed different results.

The honeycomb might be more effective at quenching the growth reactions lower in the flame due to the fact that it seemed to be conducting more heat away from the particles. This excess heat conduction may have lead to easier oxidation of the particles higher in the flame, and thus the lower values than the screen quench at these locations. Another factor that points to the possibility of reactions continuing after quenching, is the fact that the temperature of the soot and gases entering the filter were seen to be dependent on the rate at which the screen was moving. However, this theory could be dispelled because the honeycomb and screen showed roughly the same temperature of collected gases while still giving different results for the flame profiles.

It must also be realized that the flame profiles taken with the soot collection system were taken without dilution of the particles and, this could have had an effect on the properties of the soot collected. But, tests with Nitrogen dilution could not be profiled because an equation for the dilution factor for the probe could not be discovered. If a proper dilution factor could be found, and percent conversion of fuel to soot could be calculated accurately for samples taken with Nitrogen dilution, the flame profiles may show different trends. One possible answer to this problem would be to modify the apparatus used by Leonard *et. al.* (1993) and then use the smoke yield equation used in those experiments.

The parts for this modification were actually ordered, but construction was never completed, so tests could not be performed. The apparatus suggested is a combination of the equipment used for these experiments, those used by Leonard *et. al.* (1993), and an added section (Figure 8). In this scheme, Nitrogen would be pumped up the sides of the inner glass tube. The flame would be quenched through the use of a screen inserted into a slot in a section added to the apparatus used by Leonard *et. al.* (1993). The soot, gases, and Nitrogen would turbulently mix through the use of a tripper plate (or mixing plate) at the top of this added section. The tripper plate is just a circular disc with an orifice in the center to induce mixing. The soot could then be collected with a probe at the top of a chimney in the experimental apparatus. The smoke yield equation could then be used to find the percent conversion of fuel to soot for this method.

One additional possibility for the higher results from the screen quenching system could be due to the sampling rate of the probe. It is usually desired to sample from a flame at roughly the same velocity the particles are moving. The velocity at the inlet of the probe was found to be 220 cm/s for a clean filter (or roughly around 2 m/s average for the collection). Velocity profiles of Flame 1 from Santoro *et. al.* (1987) show velocities of around 1 m/s at heights of about 20 mm, and velocities above 2 m/s for heights above 60 mm. Since the probe was collecting at a rate of about 2 m/s, at lower heights in the flame where the velocity is about 1 m/s, the suction of the probe may have created larger values for the soot collected. While higher in the flame, where the velocity of the probe suction and the flame are about the same, the probe would be collecting more accurately. This type of analysis may also describe some of the trends between results for collected soot from these experiments and laser scattering results.

The capabilities of the designed soot sampling system were assessed, and some possible further experimentation has been suggested. Some other experiments and modifications to the designed system could be performed to continue the study. First, a translating screen mover could be made using a translating stand. A laser type stand leg was ordered, but was not completed before the end of these experiments. The use of the translating stand would make moving the screen easier, and more constant. With the translating stand, the motion of the screen could also be automated. Another suggestion

might be to continue further studies using the honeycomb quench because it showed results closer to the laser scattering results.

This project has provided a basis for further study into the soot sampling system needed for the surface reactivity and surface area studies proposed by Santoro (1993). For these studies, larger amounts of soot will be needed (around 1 g), which might pose further problems for determining the best possible method for sampling the soot from flames. The experiments and methods outlined in this report, however, have given results that should allow for an easy continuation into possible solutions for these problems.

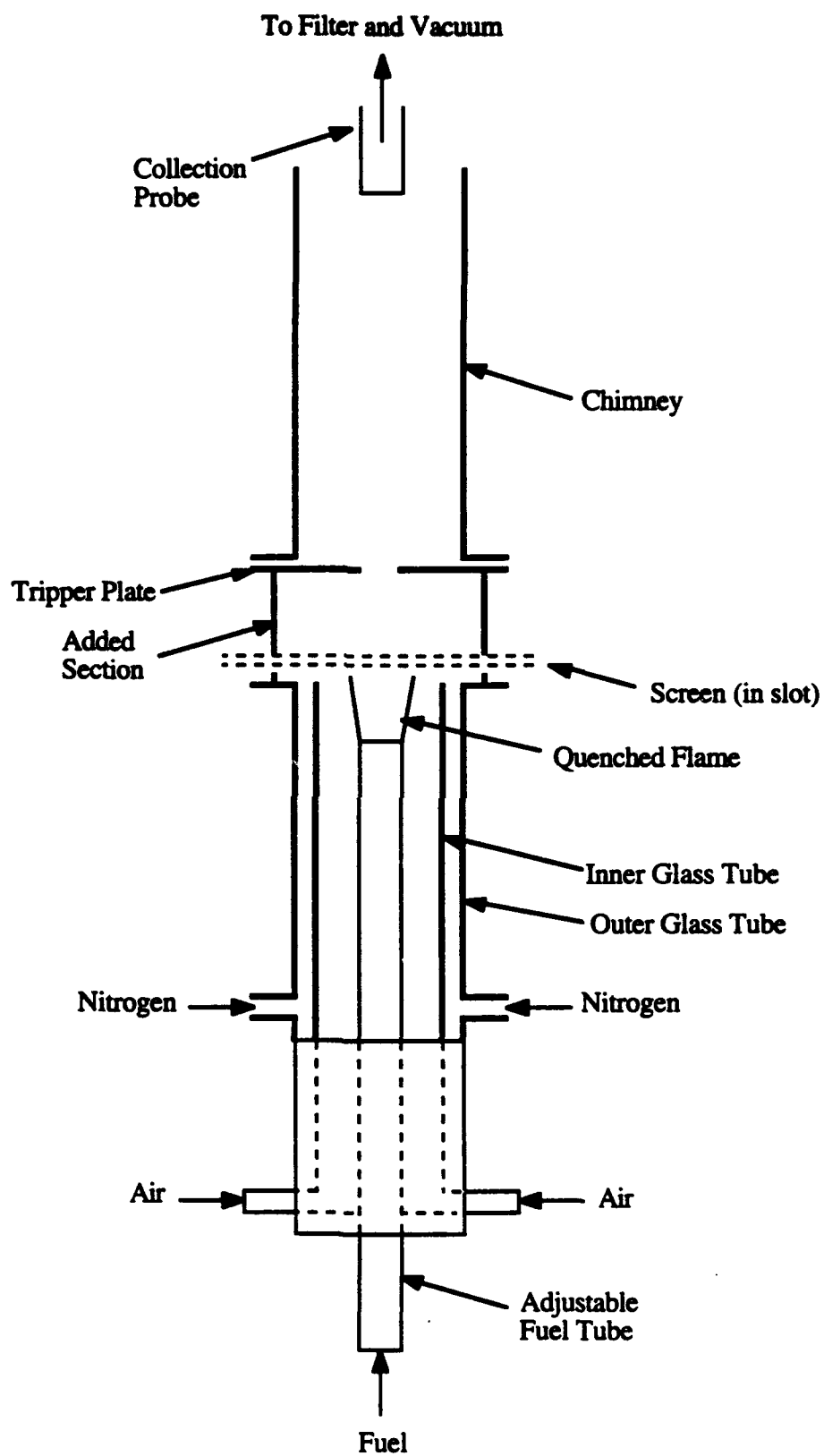


Figure 8: Alternate Soot Collection Method

APPENDIX A: Proposed Experiments and Initial Work

Proposed Methods

Initially, three different designs were proposed for soot collection systems. It was proposed to design, construct and test each of these methods to determine which system would provide the best results for the final soot collection design.

The first proposed design was to utilize the apparatus used by Leonard *et. al.* (1993), with a slight modification (Figure A1). The design used a burner with a moveable fuel tube which could be adjusted to quench different heights in the flame. The flame quenching for this system was to be performed by the use of Nitrogen dilution, which was pumped up the sides of an inner glass tube (used to constrain air flow) through an outer glass tube. The quenching was to take place at the location of a tripper plate (or mixing plate) where it was deduced that the flow of Nitrogen would be high enough to stop the

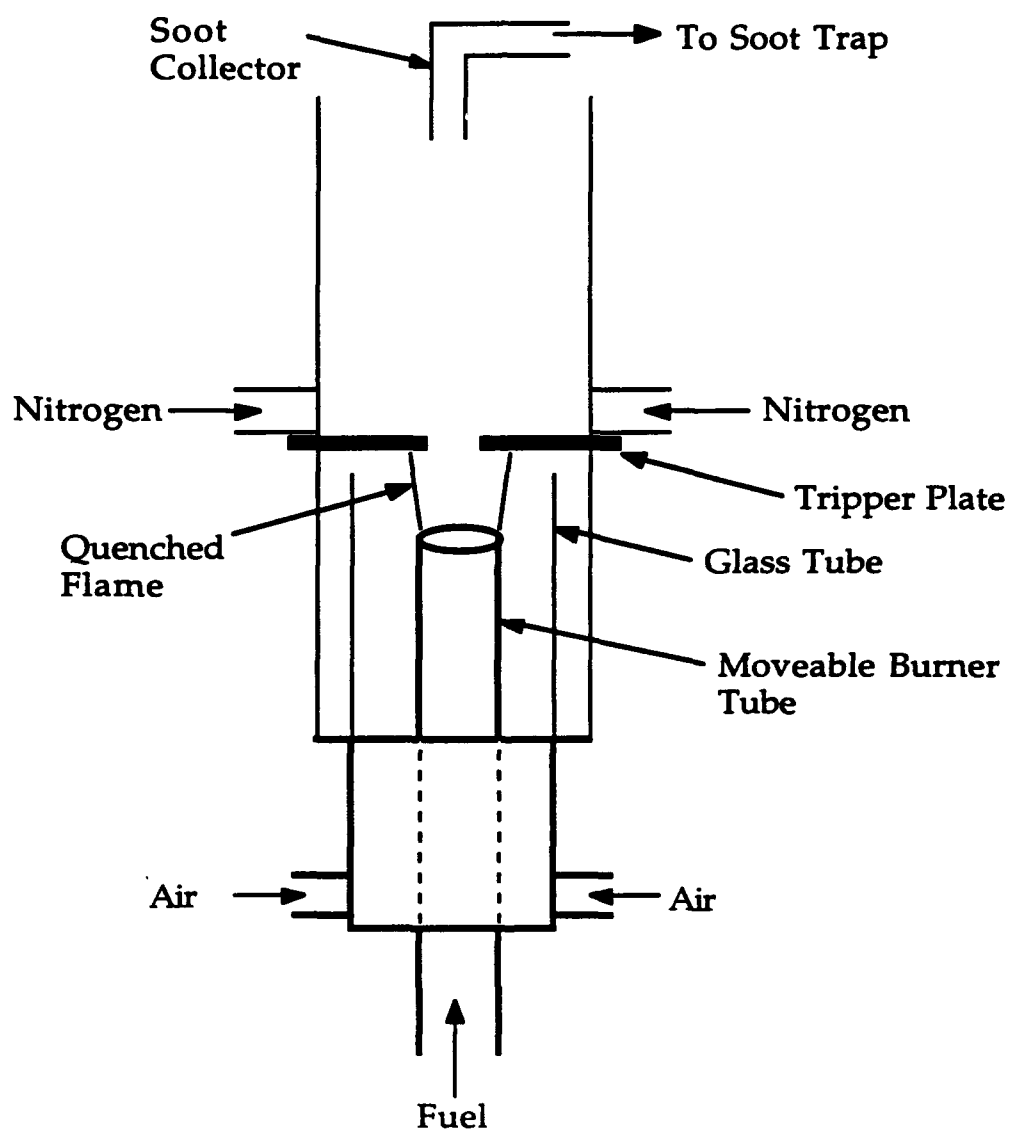


Figure A1: Proposed Tripper Plate Quenching Apparatus

flame reactions and cut the flame off at that height. The Nitrogen quenching would also serve the purpose of turbulently diluting and cooling the particles as they flowed up a chimney. The soot and gases would then be sampled through the use of a probe and filter trap connected to a vacuum line.

The second proposed method for soot collection was through the use of a dilution probe (Figure A2). For this method, a stationary burner tube could be used. The probe was to consist of two concentric tubes with the inner tube being connected to a filter holder and vacuum line for sucking up the soot and gases. Nitrogen was to be pumped through the outer tube (cooling the soot and gas sucked through the inner tube) and then turned in toward the inner tube at the inlet to the probe. This Nitrogen flow was to serve the purpose of stopping the flame reactions at the height being sampled from (quenching the flame) while at the same time diluting and cooling the soot particles.

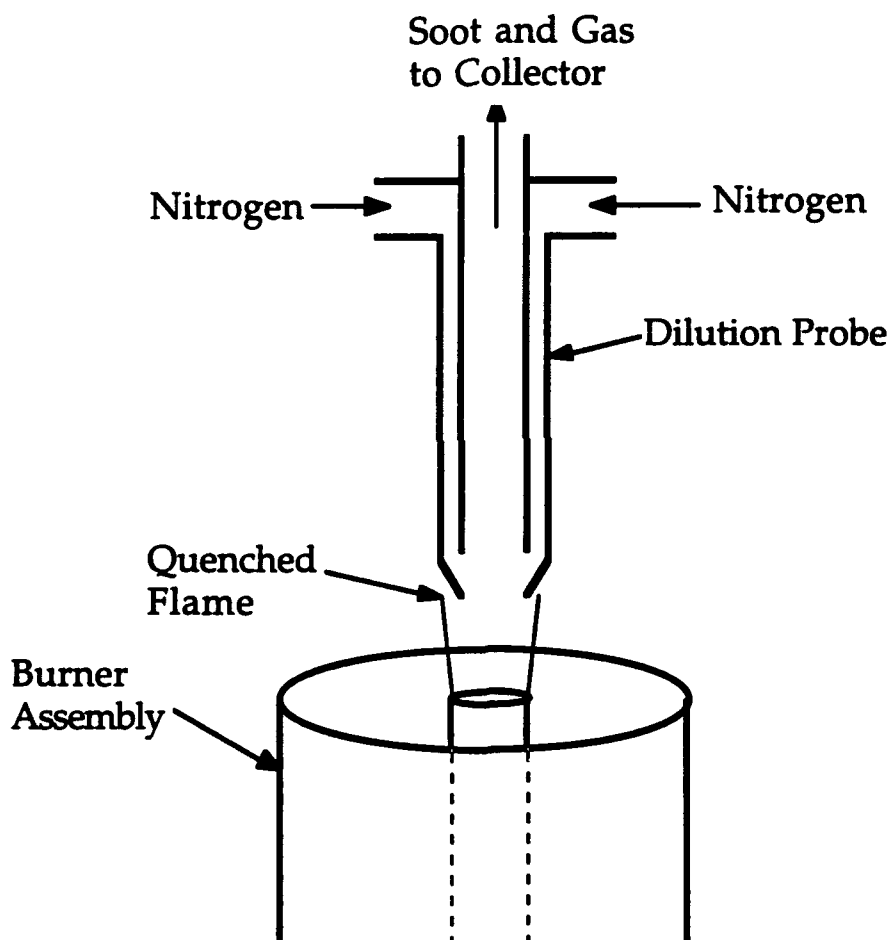


Figure A2: Dilution Probe Soot Sampling System

The last proposed design was to use a honeycomb to quench the flame, as was used in similar experiments by Roper *et. al.* (1977) (Figure A3). Nitrogen could then be immediately added to the particles and gases above the quenched flame to initialize cooling and dilution. The entire apparatus was to be connected to a vacuum line with a filter holder and filter to collect the soot.

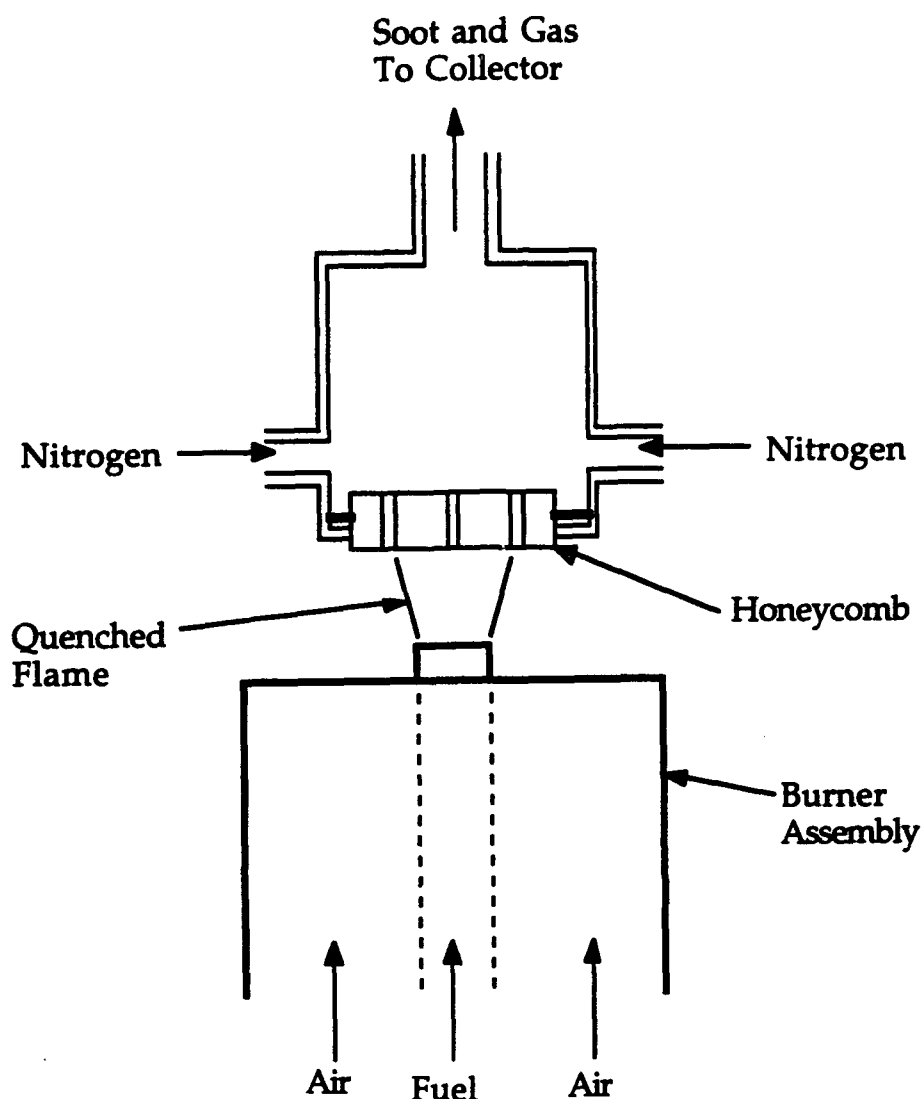


Figure A3: Honeycomb Quenching Soot Collection System

Initial Work

The first experiments attempted were on the first proposed method (tripper plate quench) because the experimental apparatus was already available. A 20 inch, 1/2 inch outer diameter, 0.032 inch thick, brass fuel tube was used for the adjustable fuel tube. A 3.85 cc/s ethylene/air overventilated laminar diffusion flame was used for these experiments. This initial experiments were attempts at determining if the tripper plate, and Nitrogen dilution would quench the flame.

The fuel tube was set so that approximately half of the flame would stick through the tripper plate (the tripper plate had an orifice diameter of 1/2 inch). The flame was ignited and allowed to stabilize. Already, the flame above the tripper plate was seen to thin out slightly due to the air and gases trying to escape through the tripper plate. As the Nitrogen flow was turned on, it was found to only thin the flame out more, and shorten it slightly above the tripper plate. Very large Nitrogen flows were attempted, but, none of them would quench the flame.

With the results of these tests, it was decided that a new tripper plate design might help to quench the flame. Several different tripper plates designs were constructed from a sheet of aluminum. The first design attempted was a smaller orifice (1/4 inch diameter), and this showed the same results as the initial tripper plate. The next design used the 1/4 inch orifice again, but this hole was surrounded by 8 1/16 inch diameter holes which were hoped to increase mixing. This tripper plate design did not show any better results than the other two. After a few more unsuccessful attempts with tripper plates designed with an orifice in the center, a tripper plate was designed that just consisted of a 1 inch square grid of 1/16 inch diameter holes. This tripper plate was found to cut the flame off (quench it) without any disturbance to the flame below the quench. However, the holes would plug with soot in a matter of seconds, which was not desired.

The idea of the grid lead to an attempt at quenching the flame using a screen. It was found that a screen worked just as well as the grid at quenching the flame and did not clog as quickly. This discovery lead to the design of the soot collection system used in this paper.

Some further tests were also performed to assess the feasibility of using Nitrogen flow to quench a flame. Two small (1/8 inch) copper tubes were connected to the Nitrogen flow. The idea behind these tubes was to determine if the Nitrogen flow would be able to cut the flame off. It was found that the Nitrogen flow would cut the flame off, but it took a very large flow rate through the tube to accomplish this without disturbing the rest of the flame. At these large flow rates, the Nitrogen flow would blow the soot from the flame in its direction which would make sampling this soot difficult. These tests helped to confirm, that a Nitrogen quenching system would be difficult to implement for the soot collection system. Since the Nitrogen quenching system was not going to work, the dilution probe would not be able to quench the flame. However, it was decided that a screen could be used to quench the flame, and the dilution probe could be used to collect and dilute the soot particles. It was decided to design a soot collection system that utilized these methods.

APPENDIX B: Rotameter Calibration

Introduction

A rotameter is a flow measurement device whose operation is based on drag principles. A rotameter consists of a tapered tube and one or more solid floats that are free to move vertically in the tube (Figure B1). Fluid entering the bottom of the tube raises the float until drag and buoyancy forces are balanced by the weight of the float (Dally, 1984). The position of the float can then be directly translated into a flow rate of the fluid moving through the tube by reading a graduated scale on the tube.

Since rotameters can be used for many different fluids each having different properties that will affect the drag of the floats, the scale used on rotameters is just a reference and does not have dimensions. For this reason, rotameters have to be calibrated to determine their response for flow conditions of the gases that they will be used for.

Experimental Procedure

For this calibration, a number 602 Matheson Gas Products rotameter flow meter was calibrated for two different gases - ethylene and methane. Also, a number 604 rotameter was calibrated for Nitrogen. The calibration for the 602 meters was performed by measuring flow rates using two different size bubble flow meters. The larger bubble meter was used to calibrate for large flow rates and had a capacity of 1000 ml with 10 ml increments. The small bubble flow meter was used for smaller flow rates and had a capacity of 100 ml with increments of 0.1 ml. A description of the method for determining the transition between the large and small bubble meters will be described in more detail later. The 604 rotameter was calibrated using a dry gas meter with a 1 liter displacement. A diagram of the general design of a bubble flow meter is shown in Figure B2. The flow meter consists of a tube marked off in some form of milliliter increments. At the base of the tube is a rubber squeeze ball, which is used to produce bubbles that will flow up the tube. Also at the base of the tube but just above the rubber ball, is a tube which provides a lead to the gas line for which the flow is to be measured.

The calibration of a rotameter using a bubble flow meter (or dry gas meter) is performed by placing the rotameter and bubble flow meter in series with the gas flow. A schematic of the experimental set up for the calibrations performed is shown in Figure B3. As can be seen from this figure, the gas to be calibrated for is supplied to the system from a cylinder and pressure regulator. The gas line from the cylinder is first connected to the rotameter, and then is connected from the rotameter to the bubble flow meter. The bubble meter is placed under an exhaust hood in order to exhaust the gas that flows out of the system from the top of the bubble meter.

One of the first steps in calibrating a rotameter is to record the atmospheric temperature and pressure, because the calibration will be slightly dependent on these factors. After the pressure was recorded, the gas cylinder was opened, and the regulator was adjusted to supply 20 psi during the calibration. Once the calibration system was pressurized, the connections from the rotameter to the bubble meter were checked for leaks using a leak detector solution. It is important that there are not any leaks in this part of the calibration system, otherwise the rotameter and the bubble meter would be experiencing different flow rates.

To begin the calibration, the inside surface of the bubble meter had to be wetted with a soapy solution. Leak detector was used to wet the sides of the bubble meter, and enough was used to ensure a good wetting of the entire surface. The excess run-off of the

leak detector collected in the squeeze ball and could be used to squeeze out bubbles to measure the flow. The first bubble meter used in this calibration was the large meter. With the bubble meter wetted, the rotameter was opened up, and a couple of bubbles were allowed to flow up the bubble meter to ensure the entire surface was wet.

The calibration was performed by first setting the rotameter at a random setting. Then, the position of the steel and pyrex floats in the rotameter were recorded. Once the rotameter readings were recorded, two bubbles were squeezed into the bubble meter. The first bubble ensured a wetted surface for the second bubble, which was used to read the flow. To record the flow with the bubble, it was timed using a stop watch, and the number of milliliters the bubble displaced was recorded. Once the time and displacement were recorded, the flow could be easily found (cc/s) by dividing the displacement by the time. In order to ensure accurate results for these flow measurements, the bubble displacement was recorded for times on the stop watch of around thirty seconds. Flow rates on the large bubble meter where the bubble would not displace 100 ml in thirty seconds were not recorded, but after recording about 10 to 15, points, these lower flow rates were calibrated using the small bubble meter. It should be noted that flow rates for rotameter readings under 20 were not recorded because the accuracy of the rotameter decreases, and a different size rotameter should be used for these flow rates. The calibration was first performed with ethylene and then methane gas.

The calibration was performed using the same method for the dry gas meter, except, the displacement of the meter was timed. The flow rate was then found by dividing the displacement by the time and then multiplying by 60 seconds. This gave a flow rate in liters per minute which could then be converted to cc/s. This calibration was performed for Nitrogen.

Once all of the data had been taken for the rotameter readings, bubble displacement, and times, the flow rates (cc/s) were calculated for each rotameter reading. Using this data, six graphs were made. One graph for each gas and for each different type of ball float read from the rotameter. In these graphs, the rotameter ball reading was plotted versus the recorded flow rate. Included in this plot was a zero point to allow for a more accurate curve fit. With the data plotted, a third order polynomial was fit to the data, and this equation could then be used as the calibration equation for the particular ball float in the rotameter, for the type of gas specified.

Results and Discussion

The calibration was performed on June 10, 1993, and the temperature and atmospheric pressure were respectively recorded as 22°C and 731.7 mm of Hg. The first gas used for the calibration was ethylene. After the system had been set up checked for leaks data points were taken using the large bubble meter. It was found that for rotameter readings below about 70 for the pyrex float, the large bubble meter was not useful for measuring the flow. The small bubble meter was used to take data points for these flow rates. After the data points had been taken for the ethylene gas, the procedure was repeated for methane.

Once all of the data had been obtained, the flow rates were calculated for each of the rotameter readings recorded. The data and calculated flows for the calibration of the rotameter for the two different gases can be found in Tables B1, B2, and B3. These numbers were then used to produce calibration curves for each type of float and each gas used. This produced four graphs which were then curve fitted using a third order polynomial. These graphs along with the calibration equations can be found in Figures B4 through B9. It should be noted the all of the calibration equations had coefficients of

correlation of 0.998 except for the steel float for ethylene which had a coefficient of correlation of 0.999.

The results of the calibration were compared to a calibration that had been performed on the same rotameter by another lab member. The comparison showed almost exact results with errors of less than 1% between the two calibrations.

Conclusion

The proper calibration of equipment before performing any experiment is important in order to ensure the accuracy of the results of that experiment. This paper outlined the general procedure for the calibration of a rotameter flow meter. An actual calibration was performed using bubble flow meters to measure flow rates, and the results of the calibration were described briefly. The results showed that the calibrations were accurate in the curve fit to the data and also when compared to a calibration previously performed on the rotameter.

List of Tables

Table B1: Calibration Data for Rotameter #602 with Ethylene Gas

Table B2: Calibration Data for Rotameter #602 with Methane Gas

Table B3: Calibration Data for Rotameter #604 with Nitrogen

List of Figures

Figure B1: General Rotameter Configuration

Figure B2: General Bubble Flow Meter Configuration

Figure B3: Rotameter Calibration Experimental Set Up

Figure B4: Ethylene Calibration Curve for Rotameter #602 Pyrex Float

Figure B5: Ethylene Calibration Curve for Rotameter #602 Steel Float

Figure B6: Methane Calibration Curve for Rotameter #602 Pyrex Float

Figure B7: Methane Calibration Curve for Rotameter #602 Steel Float

Figure B8: Nitrogen Calibration Curve for Rotameter #604 Pyrex Float

Figure B9: Nitrogen Calibration Curve for Rotameter #604 Steel Float

Rotatameter Calibration Data

32

Rotameter Type: 602
 Gas Type: Ethylene
 Temperature: 22 C
 Pressure: 731.7 mm Hg

Pyrex

Rotameter Reading	Volume Measured (cc)	Time (s)	Calculated Flow (cc/s)
145	200	24.58	8.14
75	100	29.22	3.42
135	300	40.05	7.49
85	150	35.56	4.22
120	200	30.97	6.46
100	200	39.19	5.10
115	200	33.16	6.03
80	150	38.91	3.86
130	300	41.56	7.22
105	150	27.38	5.48
90	150	32.75	4.58
20	20	35.25	0.57
65	80	28.50	2.81
30	20	21.63	0.92
55	60	27.63	2.17
40	50	36.34	1.38
50	50	26.63	1.88

Steel

Rotameter Reading	Volume Measured (cc)	Time (s)	Calculated Flow (cc/s)
74	200	24.58	8.14
35	100	29.22	3.42
68	300	40.05	7.49
41	150	35.56	4.22
59	200	30.97	6.46
49	200	39.19	5.10
56	200	33.16	6.03
38	150	38.91	3.86
65	300	41.56	7.22
52	150	27.38	5.48
44	150	32.75	4.58
60	250	38.82	6.44
110	300	24.62	12.19
80	300	33.97	8.83
135	400	25.85	15.47
45	200	43.32	4.62
100	300	26.38	11.37
145	500	30.15	16.58
115	500	38.66	12.93
125	400	28.37	14.10
30	80	28.50	2.81
24	60	27.63	2.17
21	50	26.63	1.88

Table B1

Rotameter Type: 602
 Gas Type: Methane
 Temperature: 22 C
 Pressure: 731.7 mm Hg

Pyrex

Rotameter Reading	Volume Measured (cc)	Time (s)	Calculated Flow (cc/s)
75	100	28.53	3.51
145	300	30.93	9.70
100	200	36.03	5.55
125	200	25.72	7.78
85	200	46.37	4.31
135	300	34.50	8.70
95	200	38.13	5.25
105	200	33.75	5.93
115	200	29.28	6.83
80	100	25.21	3.97
150	300	30.31	9.90
20	20	35.48	0.56
65	80	29.81	2.68
30	24	27.40	0.88
55	60	29.44	2.04
40	40	31.55	1.27
50	50	28.00	1.79

Steel

Rotameter Reading	Volume Measured (cc)	Time (s)	Calculated Flow (cc/s)
36	100	28.53	3.51
76	300	30.93	9.70
50	200	36.03	5.55
64	200	25.72	7.78
42	200	46.37	4.31
70	300	34.50	8.70
48	200	38.13	5.25
53	200	33.75	5.93
59	200	29.28	6.83
39	100	25.21	3.97
73	300	30.31	9.90
85	300	27.31	10.98
95	500	39.93	12.52
105	500	35.76	13.98
115	600	38.63	15.53
125	600	35.32	16.99
135	600	32.12	18.68
145	600	29.65	20.24
150	600	28.56	21.01
30	80	29.81	2.68
24	60	29.44	2.04
21	50	28.00	1.79

Table B2

Rotatameter Type: 604
 Gas Type: Nitrogen
 Temperature: 22 C
 Pressure: 729.22 mm Hg

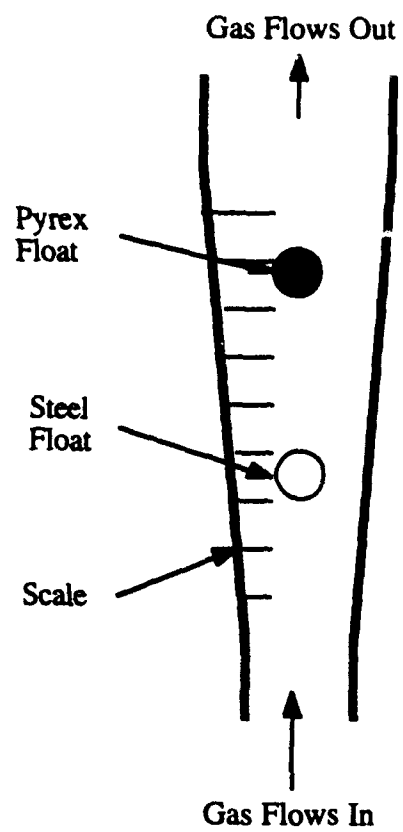
Pyrex

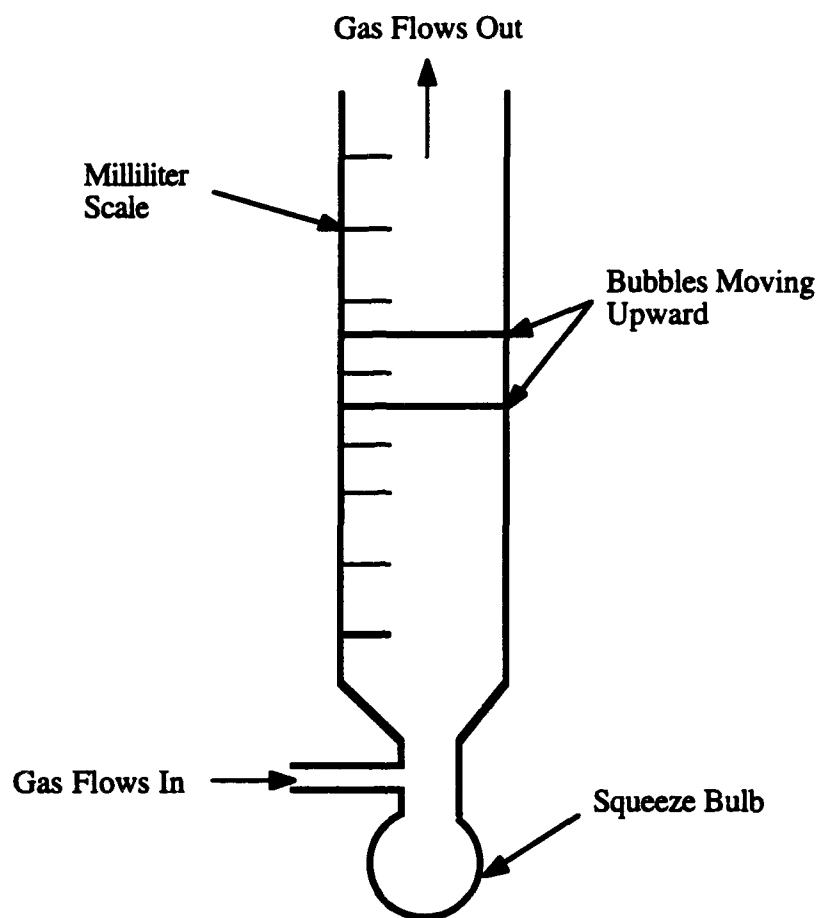
Rotatameter Reading	Volume Measured (cc)	Time (s)	Calculated Flow (cc/s)
21	1000	45.50	21.98
41	3000	69.34	43.27
60	3000	45.65	65.72
78	3000	34.63	86.63
98	3000	27.75	108.11
118	4000	31.22	128.12
138	5000	34.12	146.54
150	4000	25.12	159.24
20	1100	49.31	22.31
130	4000	28.79	138.94
30	1000	31.75	31.50
105	5000	44.03	113.56
55	2000	33.25	60.15
85	3000	32.90	91.19
125	4000	29.81	134.18
90	5000	51.60	96.90
145	4000	25.65	155.95

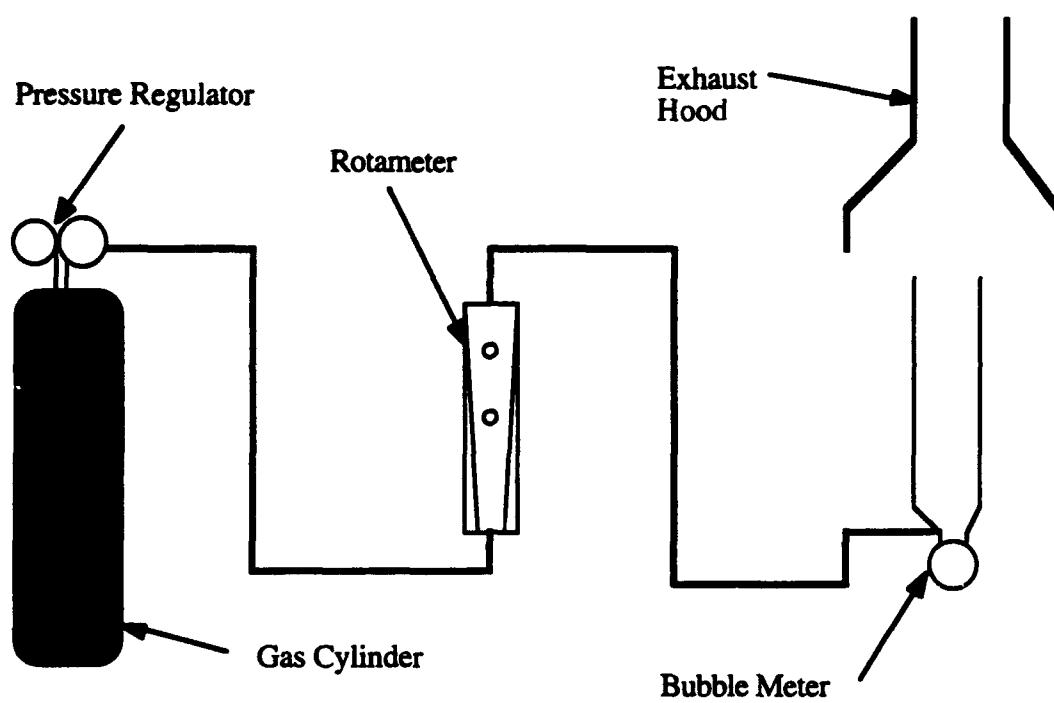
Steel

Rotatameter Reading	Volume Measured (cc)	Time (s)	Calculated Flow (cc/s)
150	10000	33.28	300.48
10	1000	45.50	21.98
140	8000	28.25	283.19
20	3000	69.34	43.27
130	8000	30.13	265.52
30	3000	45.65	65.72
120	6000	24.50	244.90
40	3000	34.63	86.63
110	6000	26.78	224.05
50	3000	27.75	108.11
100	8000	38.76	206.40
60	4000	31.22	128.12
90	6000	32.19	186.39
70	5000	34.12	146.54
80	4000	23.78	168.21
76	4000	25.12	159.24
66	4000	28.79	138.94
14	1000	31.75	31.50
53	5000	44.03	113.56
27	2000	33.25	60.15
43	3000	32.90	91.19
63	4000	29.81	134.18
45	5000	51.60	96.90

Table B3

**Figure B1**

**Figure B2**

**Figure B3**

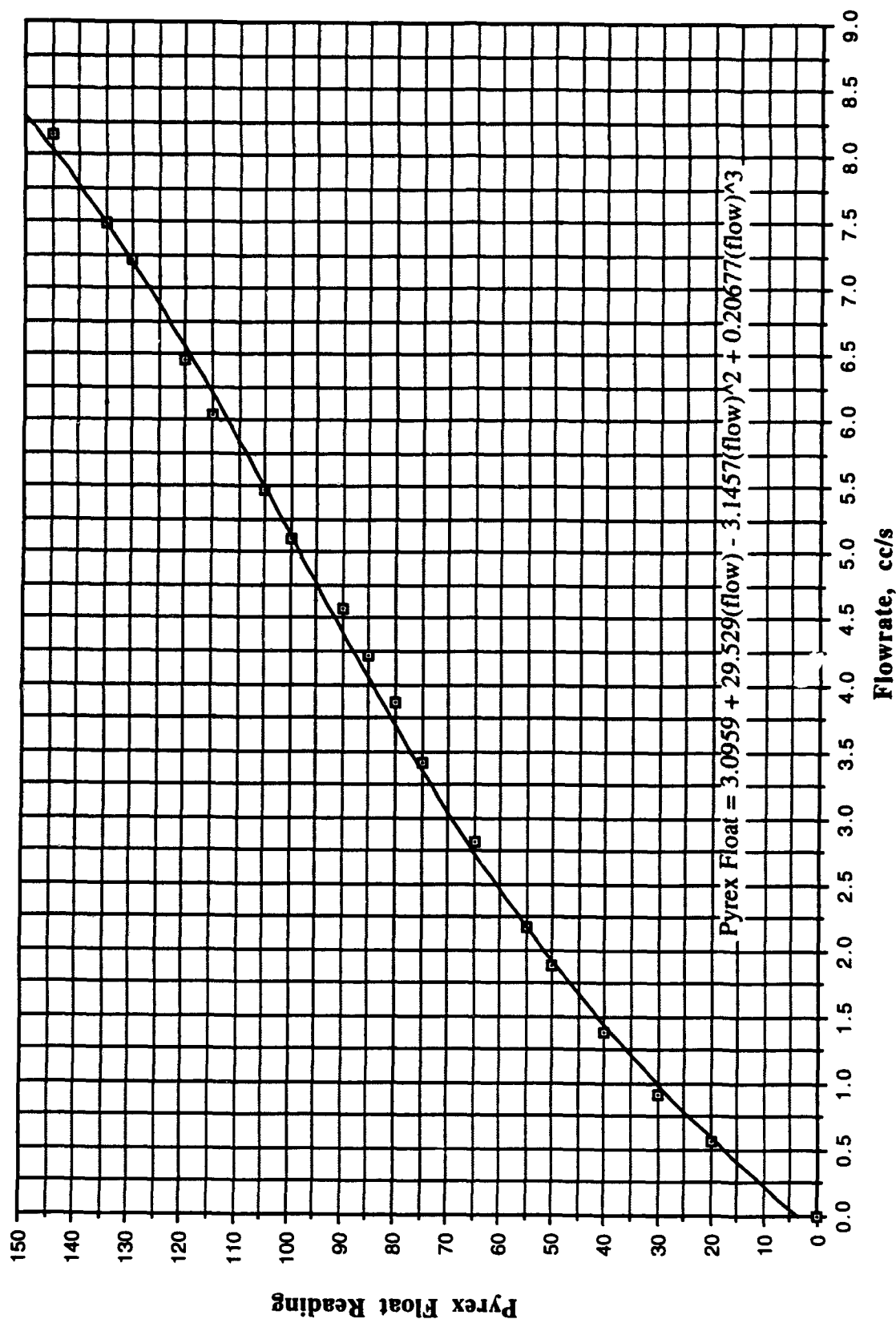


Figure B4

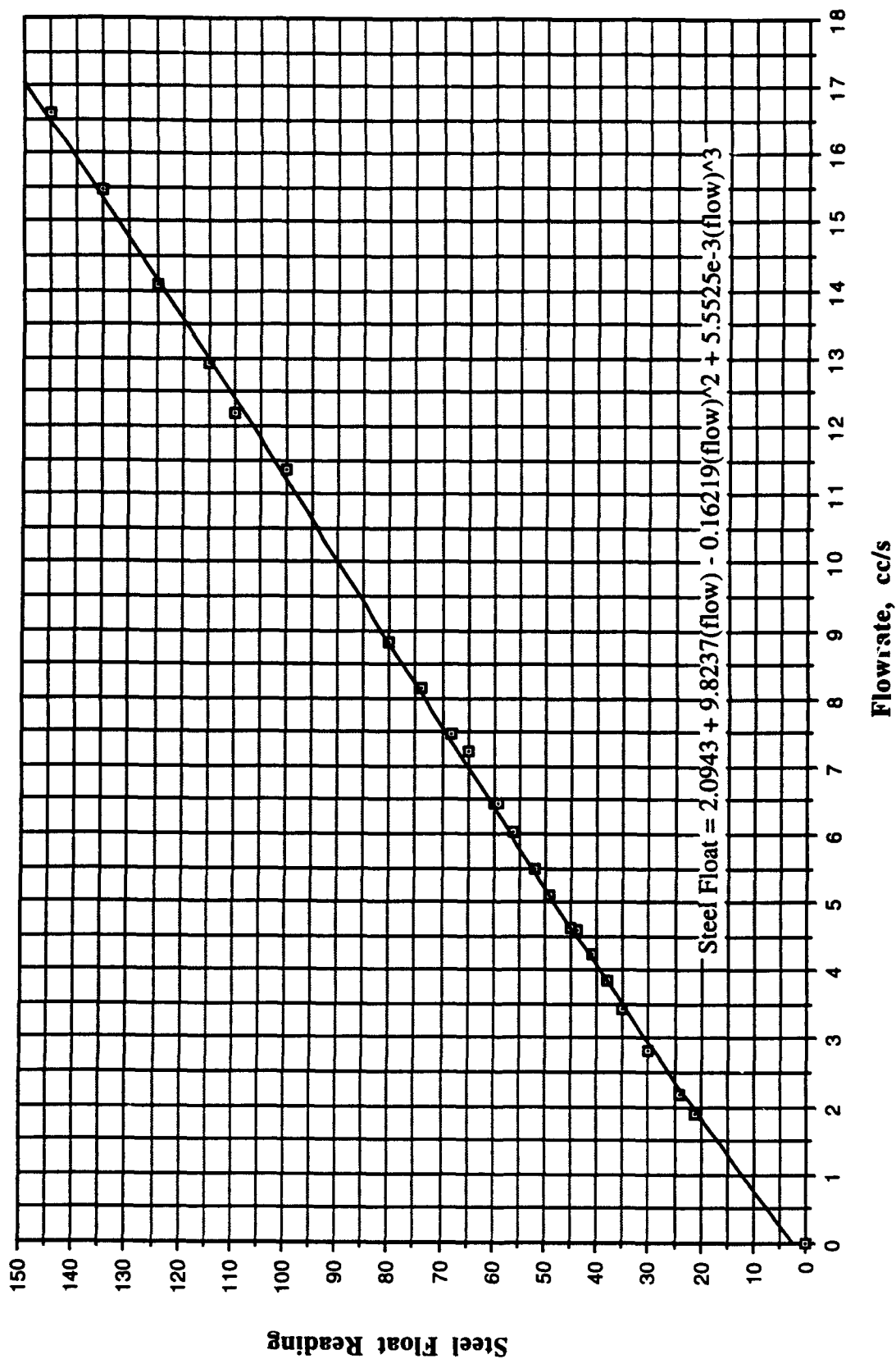


Figure B5

Rotameter #602, Methane, Pyrex Float

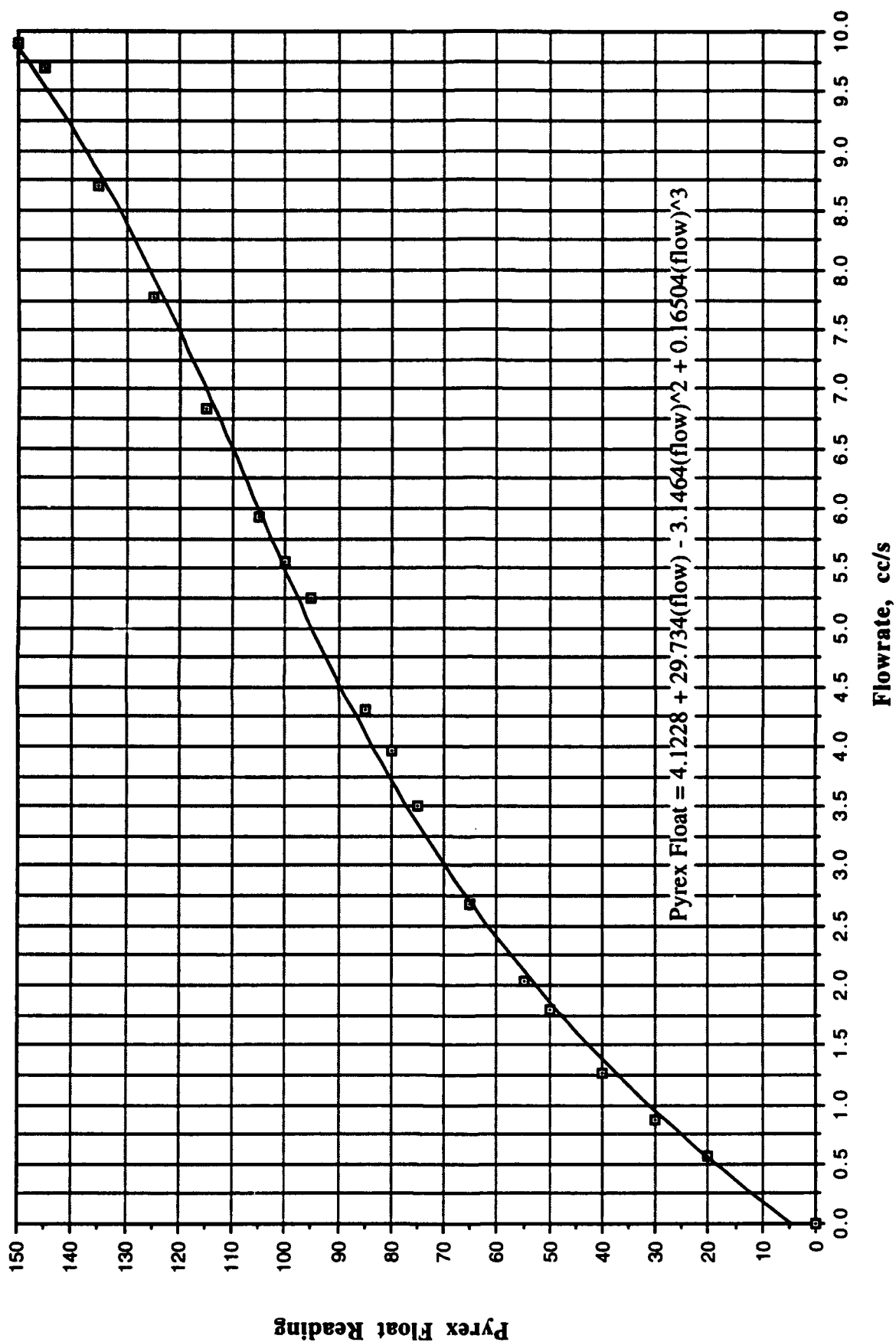


Figure B6

Rotameter #602, Methane, Steel Float

41

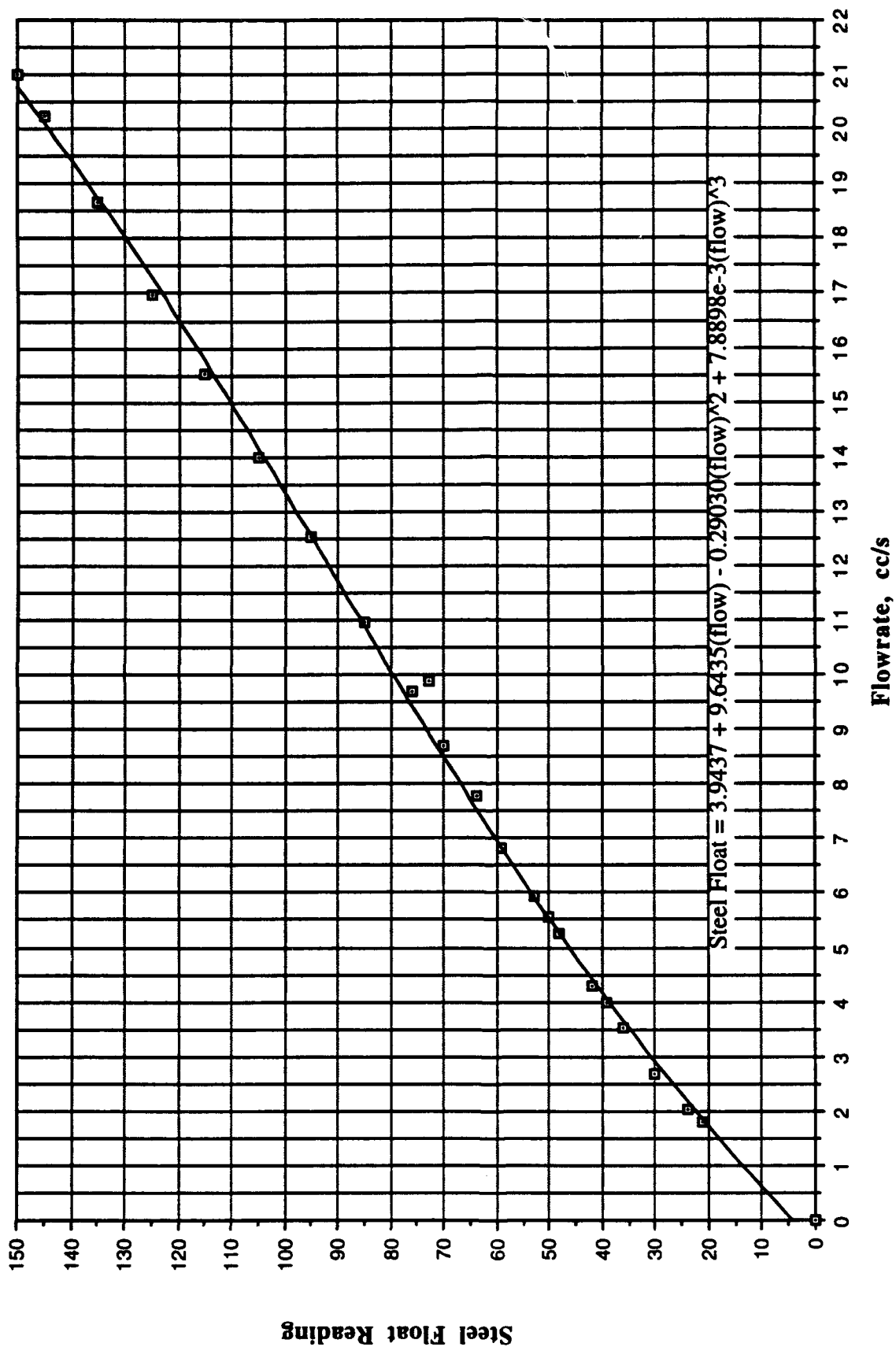


Figure B7

Calibration Curve, Nitrogen, Pyrex
Rotameter #604

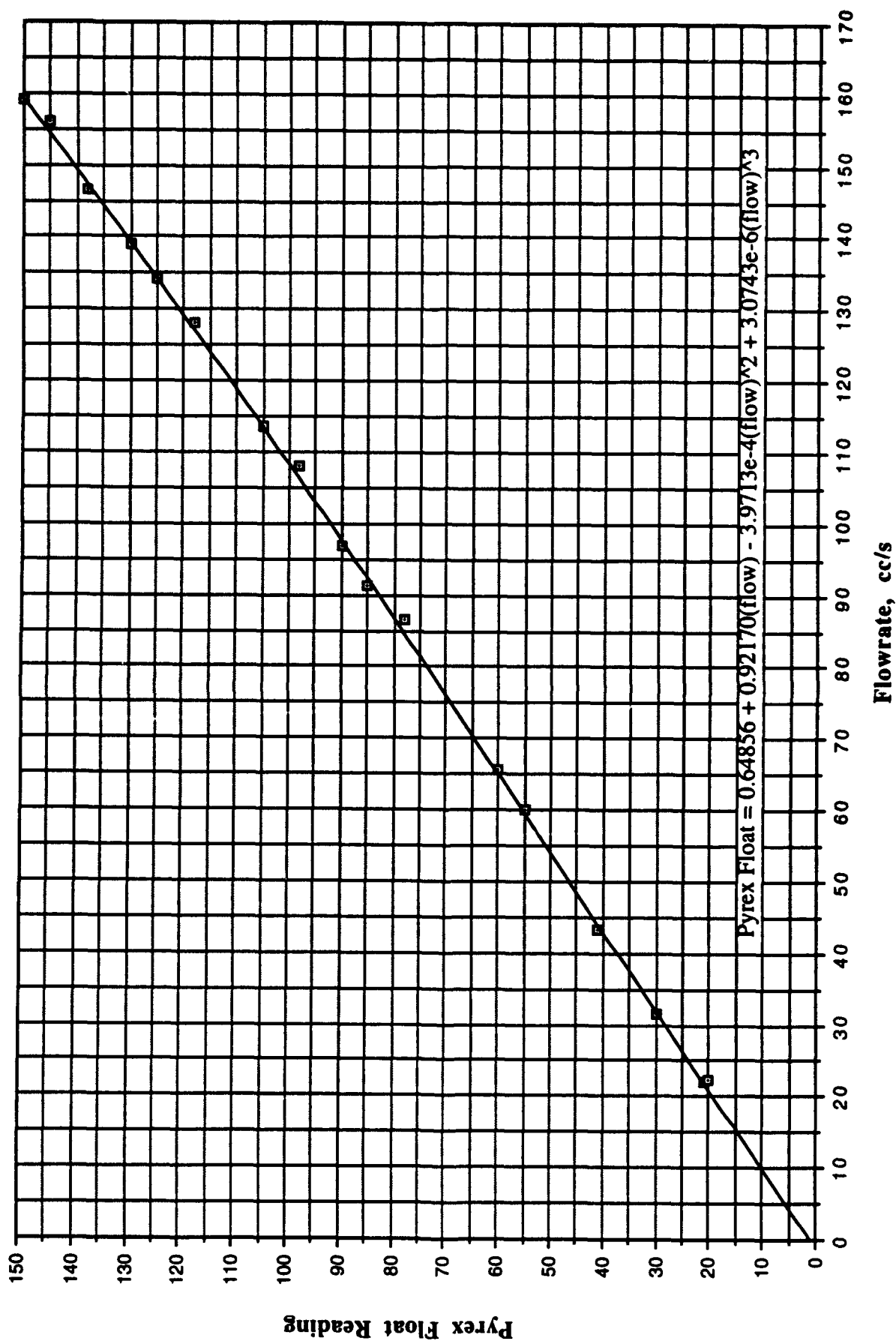


Figure B8

Calibration Curve, Nitrogen, Steel Rotameter #604

43

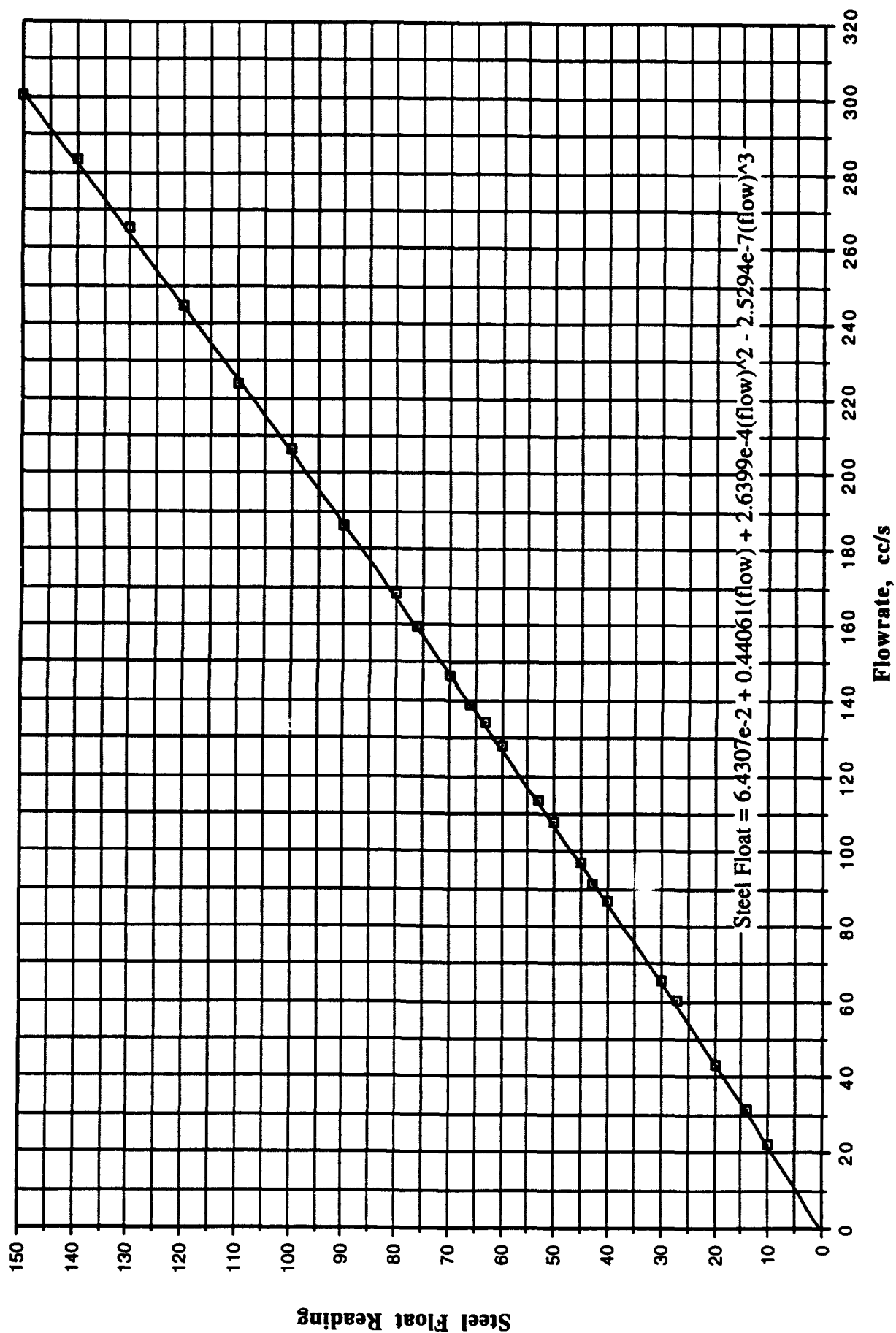


Figure B9

APPENDIX C: Tabled Data

Table C1: Flame Profile Data, Ethylene 3.85 cc/s (Trial 1), Screen Quench

Height mm	η	Soot Mass Flow $\times 10^{-4}$ (g/s)	% Conversion Fuel to Soot
2	0.0005	0.019	0.22
10	0.0027	0.413	4.71
18	0.0049	0.359	4.10
26	0.0071	1.32	15.06
34	0.0093	2.09	23.81
42	0.0115	2.09	23.81
50	0.0137	1.74	19.89
58	0.0159	1.32	15.09
66	0.0181	0.443	5.05
74	0.0203	0.104	1.18
82	0.0225	0.0	0.00

Table C2: Flame Profile Data, Ethylene 4.9 cc/s, Screen Quench

Height mm	η	Soot Mass Flow $\times 10^{-4}$ (g/s)	% Conversion Fuel to Soot
2	0.0004	0.0	0.00
14	0.0030	0.695	6.22
26	0.0056	1.29	11.56
38	0.0082	2.68	23.99
50	0.0108	2.82	25.24
62	0.0134	2.75	24.60
74	0.0159	2.21	19.76
86	0.0185	1.29	11.56
98	0.0211	0.531	4.76
110	0.0237	0.346	3.10
122	0.0263	0.083	0.74
134	0.0289	0.184	1.65

Table C3: Flame Profile Data, Ethylene 3.85 cc/s (Trial 2), Screen Quench

Height mm	η	Soot Mass Flow *10 ⁻⁴ (g/s)	% Conversion Fuel to Soot
2	0.0005	0.019	0.22
10	0.0027	0.457	5.22
26	0.0071	1.61	18.41
34	0.0093	2.15	24.51
42	0.0115	2.06	23.52
50	0.0137	1.73	19.71
58	0.0159	1.12	12.76
74	0.0203	0.1243	1.41
82	0.0225	0.0	0.00

Table C4: Flame Profile Data, Ethylene 3.85 cc/s, Honeycomb

Height mm	η	Soot Mass Flow *10 ⁻⁴ (g/s)	% Conversion Fuel to Soot
2	0.0005	0.017	0.19
10	0.0027	0.433	4.94
18	0.0049	0.960	10.95
26	0.0071	1.67	18.99
34	0.0093	1.86	21.21
42	0.0115	1.70	19.44
50	0.0137	1.43	16.31
58	0.0159	0.887	10.12
66	0.0181	0.327	3.73
74	0.0203	0.038	0.43
82	0.0225	0.0	0.00

APPENDIX D: Lubrizol Study Summary

Lubrizol is a company that manufactures oil additives, and has an interest in the experiments that are to be performed with the soot collection system. Two main projects were undertaken this summer to begin the Lubrizol study: data on fuels that will be used in the soot study, and adiabatic flame temperatures of fuel mixtures for the study.

The fuel properties were obtained from a combination of The Handbook of Chemistry and Physics, The Properties of Gases and Liquids by Reid, and an Aldrich Chemical Catalog. The fuels with corresponding properties can be seen in Table D1.

The flame temperatures were obtained using the program CEC. It should be mentioned that the enthalpies of formation for Cetane and Thiophene (Thiofuran) were obtained from Lange's Chemistry Handbook. The values were respectively -89.23 and 19.24 kcal/g-mole. The different fuel combinations and corresponding flame temperatures are summarized in Table D2.

Fuel Properties

Fuel Name	Chemical Formula	Molecular Wt. g/mol	Boiling Pt. °C	Melting Pt. °C	Density* g/ml	Viscosity* cp	Heat of Vap. g-cal/g-mol
Benzene	C ₆ H ₆	78.11	80.1	5.5	0.8765	0.652	10254.3
Cetane (Hexadecane)	CH ₃ (CH ₂) ₁₄ CH ₃	226.45	287.0	18.2	0.7733	3.340	15405.5
Decane	C ₁₀ H ₂₂	142.28	174.1	-29.7	0.7300	0.920	10339.3
2,2,4,4,6,8,8 - Heptamethylnonane	(CH ₃) ₃ CCCH ₂ CH(CH ₃) CH ₂ C(CH ₃) ₂ CH ₂ C(CH ₃) ₃	226.45	240.0	18.0	0.7930		
Isocetane (2,2,4-Trimethylpentane)	(CH ₃) ₂ CHCH ₂ C(CH ₃) ₃	114.23	99.2	-107.4	0.6919		8548.0
Methanol	CH ₃ OH	32.04	65.0	-93.9	0.7914	0.550	9377.2
Tetradecane	CH ₃ (CH ₂) ₁₂ CH ₃	198.39	253.7	5.9	0.7628		13750.0
Tert-butyl disulphide							
Thiophene (Thiofuran)	C ₄ H ₄ S	84.14	84.2	-38.2	1.0649	0.640	8748.3
Toluene (Methyl Benzene)	C ₆ H ₅ CH ₃	92.14	110.6	-95.0	0.8669	0.590	9368.5
Water	H ₂ O		100.0	0.0	0.9978	0.900	10.5 kcal

* Property at Room Temperature

Table D1

Table D2: Adiabatic Flame Temperatures
Lubrizol Study

* W = weight percentage, V = volume percent

Fuel Description	Oxidant	% Cetane*	% Toluene*	% Thiophene*	Flame Temp. (K) at		
					P = 1 atm	P = 5 atm	P = 10 atm
Pure Cetane	Air	100			2279	2319	2333
Pure Cetane	O ₂	100			3112	3334	3435
Cetane & Toluene	Air	98 W	2 W		2280	2320	2334
Cetane & Toluene	O ₂	98 W	2 W		3113	3335	3436
Cetane & Toluene	Air	90 W	10 W		2283	2323	2338
Cetane & Toluene	O ₂	90 W	10 W		3117	3339	3441
Cetane & Toluene	Air	80 W	20 W		2286	2327	2342
Cetane & Toluene	O ₂	80 W	20 W		3122	3345	3447
Cetane & Toluene	Air	70 W	30 W		2290	2331	2346
Cetane & Toluene	O ₂	70 W	30 W		3127	3351	3453
Cetane & Toluene	Air	98 V	2 V		2279	2319	2334
Cetane & Toluene	O ₂	98 V	2 V		3113	3334	3436
Cetane & Toluene	Air	90 V	10 V		2281	2321	2335
Cetane & Toluene	O ₂	90 V	10 V		3114	3336	3438
Cetane & Toluene	Air	80 V	20 V		2282	2323	2337
Cetane & Toluene	O ₂	80 V	20 V		3117	3339	3441
Cetane & Toluene	Air	70 V	30 V		2284	2325	2340
Cetane & Toluene	O ₂	70 V	30 V		3119	3342	3444
Cetane, Toluene, & Thiophene	Air	79 W	20 W	1 W	2286	2327	2342
Cetane, Toluene, & Thiophene	O ₂	79 W	20 W	1 W	3122	3346	3448
Cetane, Toluene, & Thiophene	Air	79 V	20 V	1 V	2283	2323	2337
Cetane, Toluene, & Thiophene	O ₂	79 V	20 V	1 V	3117	3339	3441

Equiv. Ratio = 1.0 for all cases

REFERENCES

- Burke, S.P. and T.E.W. Schumann. *Industrial Engineering and Chemistry*, 1928, Vol. 20, pp. 998-1004.
- Dally, James W. Instrumentation For Engineering Measurements. John Wiley & Sons, Inc., 1984.
- Frenklach, Michael and Hai Wang. "Detailed Modeling of Soot Particle Nucleation and Growth," *Twenty-Third Symposium (International) on Combustion*. The Combustion Institute, 1990, pp. 1559-1566.
- Glassman, Irvin. Combustion, 2nd Edition. Academic Press, 1987.
- Harris, Stephen J. and Anita M. Weiner. "Surface Growth of Soot Particles in Premixed Ethylene/Air Flames," *Combustion Science and Technology*, 1983, Vol. 31, pp. 155-167.
- Leonard, S., G.W. Mulholland, R. Puri and R.J. Santoro. "Generation of CO and Smoke During Underventilated Combustion," Department of Mechanical Engineering, The Pennsylvania State University, 1993.
- Liu, B.Y.H., D.Y.H. Pui and K.L. Rubow. *Aerosol in the Mining and Industrial Work Environment, Vol. 3, Instrumentation*, (V.A. Marple and B.Y.H. Liu, Eds.) Ann Arbor Science, The Butterworth Group, 1983.
- McKinnon, Julian T. Jr. "Chemical and Physical Mechanisms of Soot Formation," Ph. D. Thesis, Massachusetts Institute of Technology, 1989.
- Santoro, R.J., T.T. Yeh, J.J. Horvath and H.G. Semerjian. "The Transport and Growth of Soot Particles in Laminar Diffusion Flames," *Combustion Science and Technology*, 1987, Vol. 53, pp. 89-115.
- Santoro, R. J. Research Proposal, 1993.
- Wieschnowsky, U., H. Bockhorn and F. Fetting. "Some New Observations Concerning the Mass Growth of Soot in Premixed Hydrocarbon-Oxygen Flames," *Twenty-Second Symposium (International) on Combustion*. The Combustion Institute, 1988, pp. 343-352.
- Woods, I. T. and B.S. Haynes. "Brief Communication: Soot Surface Growth at Active Sites," *Combustion and Flame*, 1991, Vol. 85, pp. 523-525.
- Zucrow, Maurice J. and Joe D. Hoffman. Gas Dynamics. John Wiley and Sons, Inc., 1976.

Attachment B

**Spatially Resolved Measurements of Soot Volume Fraction
Using Laser-Induced Incandescence**

Spatially Resolved Measurements of Soot Volume Fraction Using Laser-Induced Incandescence

B. QUAY, T.-W. LEE, T. NI, and R. J. SANTORO*

Department of Mechanical Engineering, The Pennsylvania State University, University Park, PA 16802

Laser-induced incandescence is used to obtain spatially resolved measurements of soot volume fraction in a laminar diffusion flame, in which comparisons with laser scattering/extinction data yield excellent agreement. In addition, the laser-induced incandescence signal is observed to involve a rapid rise in intensity followed by a relatively long (ca. 600 ns) decay period subsequent to the laser pulse, while the effect of laser fluence is manifest in nonlinear and near-saturated response of the laser-induced incandescence signal with the transition occurring at a laser fluence of approximately 1.2×10^8 W/cm². Spectral response of the laser-induced incandescence involves a continuous spectrum in the visible wavelength range due to the blackbody nature of the emission. Simultaneous measurements of laser-induced incandescence and light scattering yield encouraging results concerning the mean soot particle diameter and number concentration. Thus, laser-induced incandescence can be used as an instantaneous, spatially resolved diagnostic of soot volume fraction without the need for the conventional line-of-sight laser extinction method, while potential applications in two-dimensional imaging and simultaneous measurements of laser-induced incandescence and light-scattering to generate a complete soot property characterization are significant.

INTRODUCTION

Formation, growth, and oxidation of soot particles in diffusion flames involve a complex interaction between chemistry and fluid mechanics. The understanding of these chemical and physical processes is important not only from a fundamental scientific standpoint, but also due to their applications in practical combustion devices. For example, soot emission from automotive and gas turbine engines constitutes one of the major pollutants that needs to be minimized, while excessive soot formation and radiation in propulsion devices have adverse effects on combustor and flow components. In this regard, sooting characteristics of both turbulent and laminar flames have been investigated by numerous researchers, while in this laboratory attention has been focused on axisymmetric laminar diffusion flames. The soot property measurements made in this flame, thus far, involve the laser scattering/extinction method. This technique yields measurements of soot volume fraction, mean soot particle

diameter, and number density after tomographic inversion of the laser extinction data due to the line-of-sight nature of these measurements.

However, recent studies of a process involving laser-induced incandescence (LII), in which the soot particles are heated up by the laser energy and emit blackbody radiation or incandescence at elevated temperatures, have shown that LII can be used as a nonintrusive spatially resolved soot diagnostic [1-6]. In particular, it has been pointed out by Melton [1] that the LII signal is nearly proportional to the local soot volume fraction for sufficiently large laser fluence; thus, a pointwise measurement of soot volume fraction can be made without the need for the line-of-sight laser extinction and time-consuming tomographic inversion method. While other applications of LII in soot diagnostics, for measurements of soot particle size distribution for example, have been suggested [1], the most direct and significant application of LII may be in obtaining point measurements of soot volume fraction since the line-integral nature of laser extinction and subsequent tomographic inversion technique have deficiencies in some laminar flame and most

*Corresponding author.

turbulent flame configurations. For example, instantaneous measurements of local soot volume fraction can be made in turbulent diffusion flames using LII without being limited to time-averaged data or an axisymmetric burner geometry. Furthermore, applications of LII in investigations of soot properties include two-dimensional imaging of soot volume fraction distributions and simultaneous LII and scattering measurements to construct a complete soot property characterization. Recently, qualitative information on soot formation under Diesel engine conditions have been reported in which simultaneous two-dimensional LII and light-scattering images were obtained [5, 6].

In spite of these potentially significant applications of LII in soot diagnostics, no experimental verification of the LII technique for determining the local soot volume fraction has been reported to date. The objectives of this investigation, therefore, were to experimentally determine the applicability of the LII method to obtain spatially resolved measurements of soot volume fraction, to study the feasibility of making simultaneous LII and light-scattering measurements to obtain a complete soot property characterization, as well as to investigate the detailed characteristics of LII in laminar diffusion flames.

LASER-INDUCED INCANDESCENCE

Laser-induced incandescence involves the heating of soot particles to temperatures above the surrounding gas temperature due to the absorption of laser energy, and subsequent detection of the blackbody radiation corresponding to the elevated soot particle temperature. The temperature of the soot particle is determined by the rate of laser energy absorption, conductive heat transfer to the surrounding gas, soot vaporization, and radiative heat loss through blackbody radiation [1, 2]. For example, a Nd:YAG pulsed laser beam of ca. 7 ns duration used in the present LII measurements represents an energy source in the energy balance equation, and the soot particle temperature rapidly rises during the duration of the laser pulse as the soot particles absorb the laser energy. The heat sink terms in this

phase are the conductive and radiative heat losses to the surrounding gas, which are much smaller than the laser energy absorption rate for laser fluence levels relevant to LII. Near a soot particle temperature of ca. 4000 K, which is close to the soot vaporization point, the temperature rise is severely curtailed by the energy expended in the vaporization of soot particles [1], although soot surface temperatures as high as 5000 K have been observed for sufficiently large laser fluence [7]. Subsequent to the laser pulse, the temperature of the soot particles gradually decreases due to conductive and radiative heat losses.

The intensity of the LII, or the blackbody radiation due to laser heating, for a single soot particle has a dependence on the soot particle temperature, detection wavelength, and the laser fluence. The total incandescence emitted from the soot particle surface has a fourth-order dependence on the soot particle temperature. The spectral shape of the incandescence is determined by Planck's law with the maximum in the blackbody radiation occurring at a wavelength inversely proportional to the soot particle temperature according to Wien's displacement law. Thus, the temporal variation in the LII signal at a given detection wavelength qualitatively follows the soot particle temperature in time, with the exact functional relationship determined by the processes described above.

Computations of the LII in response to an idealized laser pulse based on the above blackbody radiation laws and the soot particle energy balance have been performed by Melton [1] and Tait and Greenhalgh [4]. In particular, in the limit of high laser power and maximum soot particle temperature near its vaporization point, Melton [1] has shown that the intensity of the LII signal for a group of soot particles has a dependence on mean soot particle diameter raised to the power of $(3 + 0.154\lambda_{\text{det}}^{-1})$, where λ_{det} is the detection wavelength expressed in microns. For λ_{det} between 0.7 and 0.4 μm , for example, the LII signal is proportional to the mean soot diameter raised to the power of 3.22 to 3.38, or approximately to the soot volume fraction. This forms the basis for the current approach of using LII for pointwise measurement of soot volume fraction.

EXPERIMENTAL METHODS

The experimental apparatus involved a coannular laminar diffusion flame burner that was identical to the burner employed in this laboratory in previous studies of soot properties [8-10]; thus, only a brief description will be given here. The overventilated laminar flame burner consisted of two concentric brass tubes with fuel and air flowing through the inner (11.1 mm i.d.) and outer (101.6 mm i.d.) tubes, respectively, where the fuel tube extended 4 mm beyond the exit plane of the air tube. Flow conditioning for the air was achieved via a layer of 3.0-mm glass beads, a series of wire screens and ceramic honeycomb section, while the fuel passage contained a layer of 3.0-mm glass beads and a single wire screen. A 405-mm long brass cylinder that fit over the outer tube was used as a chimney to shield the flame from laboratory air disturbances; and optical access was obtained through machined slots on the brass cylinder which traversed with the burner assembly. In addition, screens and a flow restrictor were placed at the chimney exit to achieve a highly stable flame similar to previous studies [8-10]. The traverse system involved a stepper motor and controller (Daedal PC-410-288) that provided positioning capability with a resolution of 0.0127 mm.

The optical setup for the LII included an Nd:YAG pulse laser (Continuum Model NY61-10), the output beam of which was ca. 7 ns in duration and was focused to approximately 0.38 mm in diameter using a bi-convex lens of 400 mm focal length. The probe volume location was displaced ~ 25 mm from the focal point of the lens in order to achieve this 0.38 mm diameter. A schematic of the optical arrangement is shown in Fig. 1. Both the 1064-nm and frequency-doubled 532-nm beams from the Nd:YAG laser were used, the diameter of which prior to the focusing lens was approximately 9 mm with a nearly Gaussian profile. In order to observe the effect of varying the laser fluence for the 532 nm wavelength, a combination of a half-wave plate, mounted in a rotation stage, in series with a polarizing beam splitter was used to attenuate the laser energy by a varying amount. A neutral density filter (0.7 N.D.) preceded the half-wave plate to re-

duce the laser power to an acceptable value. By rotating the half-wave plate to vary the ratio of vertically polarized to horizontally polarized light, in conjunction with aligning the beamsplitter to transmit only the vertically polarized portion of the beam, laser energies ranging from 0.2 to 3.3 mJ were obtained corresponding to laser fluences between 2.5×10^7 and 4.2×10^8 W/cm². The laser energy was monitored during the experiment using a pyrometer (Molelectron J1000), and was maintained during the actual measurements of the soot volume fraction at 2.4 mJ for a laser fluence of 3.0×10^8 W/cm² in order to minimize the effect of laser beam attenuation across the flame (see discussion below). The LII signal was collected at a 90° angle using a focusing lens with an *f*-number of 3 at unit magnification. Except for the spectral scans, an interference filter (400 ± 10 nm) was placed in front of the monochromator to minimize interference from light scattering. For the spectral scans, the interference filter was removed from in front of the monochromator and the 1064-nm wavelength laser probe beam was used to produce the LII signals. For these measurements, a series of neutral density filters were used to vary the laser fluence rather than the half-wave plate/beam splitter arrangement used with the 532-nm wavelength laser probe beam.

Since the LII signal had a continuous spectrum in the visible wavelength range, while

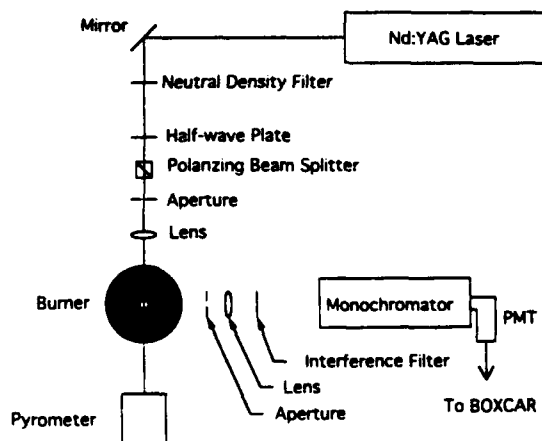


Fig. 1. Optical arrangement for laser-induced incandescence measurements.

interference from light-scattering and PAH fluorescence was expected near wavelengths of 532 nm and above [10, 11], the detection of the LII signal was made at a wavelength of 400 nm for both 532- and 1064-nm wavelength probe laser beams. Measurements made at 500- and 700-nm detection wavelengths for the 1064 nm wavelength probe laser yielded identical results due to the continuous nature of the LII spectrum in the visible wavelength range. The detection wavelength was set by using a 0.25-m monochromator (Instruments SA H20) with a grating blazed at 330 nm with 1 mm \times 1 mm slits, which also defined the length on the probe volume. The bandpass of the monochromator was estimated to be 4 nm FWHM, while the spectral response of the monochromator was calibrated using an incandescent lamp (Eppley T24). A photomultiplier tube (Hamamatsu R928) was connected to the exit slit of the monochromator, the signal from which was conditioned using a boxcar integrator with a gate width of 10 ns and averaged over 100 laser shots.

Temporal variations of the LII signal were observable by moving the boxcar gate in 2–10-ns increments. LII profiles across the flame and spectral characteristics of the LII signal were observed by using the burner traverse system described above and by the scanning of the detection wavelength via the monochromator, respectively. The measurements were made in nonsmoking ethylene/air diffusion flames where the ethylene and air flow rates were 3.85 cm³/s and 1060 cm³/s, respectively.

RESULTS AND DISCUSSION

Figure 2 shows a typical temporal variation of the LII and vertically polarized light-scattering signals taken at a height of 40 mm above the fuel tube exit for an ethylene laminar diffusion flame at the radial location where the peak soot volume fraction is observed ($r = 2.5$ mm). The variation of the LII signal in time has been obtained by increasing the boxcar gate delay in 2–10-ns increments with respect to the laser pulse while averaging over 100 laser shots, as described above. It can be observed in Fig. 2 that the initial phase of the signal involves a

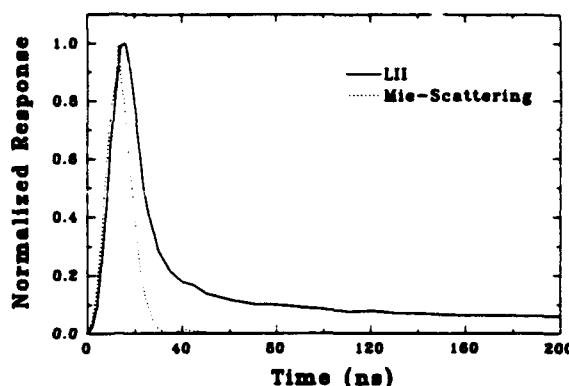


Fig. 2. Temporal response of the laser-induced incandescence.

rapid rise in the LII signal intensity due to the increase in the soot particle temperature during the laser pulse of ca. 7 ns in duration. Subsequent to the peak in the LII signal, the soot particles undergo conductive and radiative heat loss to the ambient gas and the LII signal gradually decreases, although a sensible LII signal is still observed at approximately 600 ns after the laser pulse. The temporal variation of the LII signal shown in Fig. 2 is qualitatively very similar to the LII response function for an idealized laser pulse computed by Melton [1]. A characteristic time constant for the LII process for soot particles has been shown to be linearly proportional to the soot particle diameter [3], and is estimated to be approximately 700 ns for a diameter of 100 nm. The decay time observed in Fig. 2 is approximately 600 ns for the signal to decrease to 5% of the peak value, while the mean soot particle diameter (D_{63}) at this location is approximately 135 nm (see Fig. 7b). Thus, in contrast to the light-scattering signal, which is observable in principle only during the duration of the laser pulse due to its elastic scattering nature, the LII signal exhibits a much longer temporal characteristic, as shown in Fig. 2. Melton [1] has discussed the potential for obtaining particle size distribution parameters from the temporal behavior of the LII signal. Such information is better obtained using a shorter probe laser wavelength than that used in the present study and may also suffer from interference from laser-influenced fluorescence from PAH species [1].

A comparison between the soot volume fraction measured by LII and the laser scattering/extinction technique is shown in Figs. 3a-3c, where the soot volume fraction is plotted as a function of radial location at selected heights ranging from 10 to 70 mm above the fuel tube exit. The open and dark symbols represents laser scattering/extinction and LII data, respectively. The laser scattering/extinction data for soot volume fraction in this flame has been taken from Santoro et al. [8, 9], and involves the well-known method of measuring the line-of-sight extinction of the laser beam followed by a tomographic inversion in order to reconstruct the local soot volume fraction. Further details of this technique and the data can be found in Santoro et al. [8, 9]. In order to calibrate the observed LII signal, the LII signal at a single spatial point corresponding to the radial location where the peak soot volume fraction occurs ($r = 2.5$ mm) at the 40 mm height has been equated with the known value of soot volume fraction at this location from the laser scattering/extinction measurements. All other LII data can then be converted to absolute soot volume fraction based on this single-point calibration procedure.

The radial profiles of soot volume fraction obtained in this manner, as shown in Figs. 3a-3c, exhibit the familiar physics of soot growth and oxidation in this flame. At low heights, soot particles are observed in the annular region on the fuel-rich side of the flame. Soot formed in this region undergoes net growth with increasing height up to $H = 40$ mm where the peak soot volume fraction is observed at a radial location of 2.5 mm from the centerline, while soot is observable at the centerline at a height of 30 mm in Fig. 3a. Subsequent development involves a net destruction of soot particles through soot oxidation with soot volume fraction in the annular region diminishing more rapidly than in the central region.

Figures 3a-3c show an excellent agreement between the LII and laser extinction/scattering data for the soot volume fraction with data being within 5%-10% of one another at most of the heights where measurements have been obtained. However, there is a tendency for the LII data to underestimate the soot volume

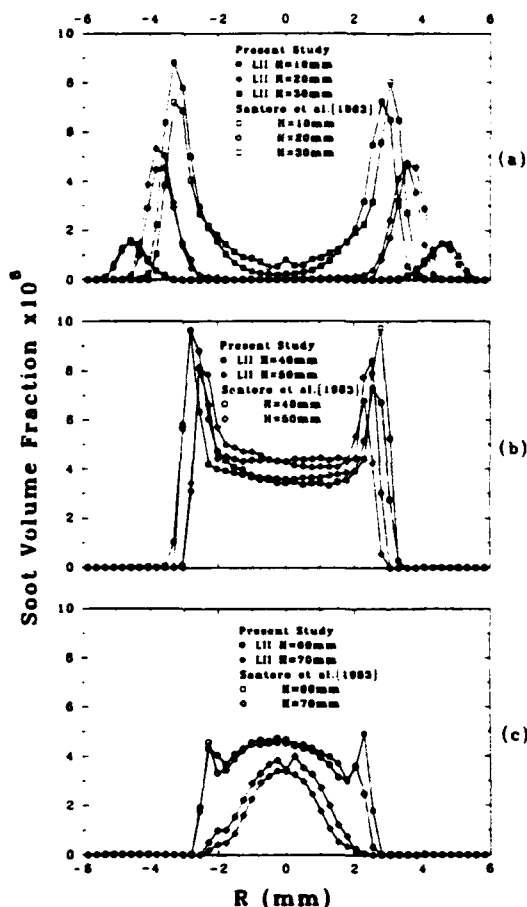


Fig. 3. Radial profiles of the soot volume fraction obtained via laser-induced incandescence and laser scattering/extinction at several heights (H) above the fuel tube exit of the burner (a) $H = 10, 20$, and 30 mm; (b) $H = 40$ and 50 mm; and (c) $H = 60$ and 70 mm.

fraction on one side of the flame, resulting in slightly asymmetric soot volume fraction profiles in Fig. 3b. This effect is more pronounced at the height of 40 mm than elsewhere and is attributable largely to the fact that the LII signal from the far soot peak traverses the flame in order to arrive at the signal detection site and, thus, is subject to increased path length and correspondingly increased absorption of the signal by the soot and PAH species in the flame. This effect may be correctable by estimating and integrating the local extinction of the signal across the flame. Figure 4 similarly shows the integrated soot volume fraction as a function of height. The comparison between the LII and laser extinction/scattering data [8, 9] yields reasonably good agreement

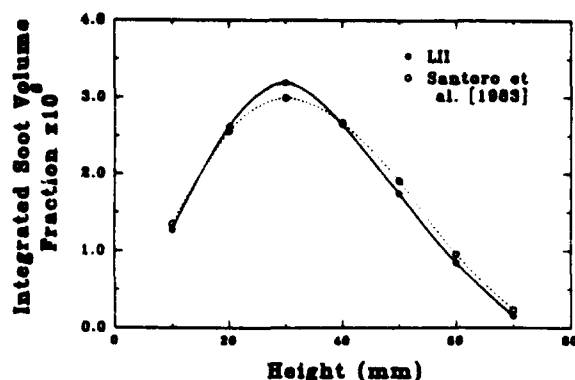


Fig. 4. Integrated soot volume fraction plotted as a function of height above the fuel tube exit of the burner.

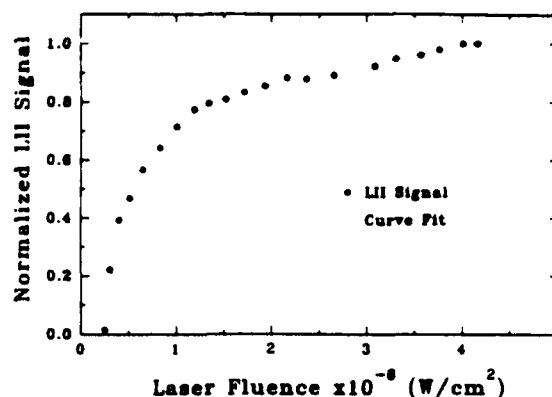


Fig. 5. Effect of laser fluence on the laser-induced incandescence signal.

with the maximum discrepancy being approximately 10% at a height of 30 mm.

The effect of laser fluence on the LII signal is shown in Fig. 5. The laser fluence has been varied from 2.5×10^7 to 4.2×10^8 W/cm² using the combination of the half-wave plate and beamsplitter, as described earlier. For a laser fluence from 2.5×10^7 to 1.2×10^8 W/cm², it can be seen in Fig. 5 that the LII signal increases rapidly as the laser fluence increases. This effect is due to the fact that the soot particle temperature increases as a function of the laser fluence, which causes a corresponding increase in the LII signal. In contrast, the LII signal for laser fluence beyond ca. 1.2×10^8 W/cm² exhibits a small increase with respect to an increase in the laser fluence. The influx of laser energy on the soot particles can cause vaporization of small carbon fragments, such as C₂ and C₃, from the soot particle surface. For sufficiently large laser fluence this vaporization mechanism and corresponding mass loss can become the dominant effect which limits the increase in soot particle temperature and, thus, causes a leveling of the LII signal as shown in Fig. 5. However, the LII signal intensity in this "saturation" regime increases as a weak function of the laser fluence in Fig. 5 similar to the results of Eckbreth [7] in which soot surface temperatures as high as 5000 K were observed with increasing laser fluence. From the data shown in Fig. 5, it is estimated that the "saturation" regime for the LII signal occurs for laser fluences above 1.2×10^8 W/cm² in the present studies. During the actual measurements of soot volume frac-

tion, large laser fluence levels in the "saturation" regime, as were used in the present study, have the advantage of being least affected by the effects of the laser beam attenuation across the flame, since the LII signal is a weak function of the laser fluence in this regime. For the results reported here, the LII response varied by less than 5% for the range of laser fluence attenuations (~30% maximum attenuation) encountered in the present study. The observed response of the LII signal to the laser fluence is sensitive to the laser beam intensity profile, the specific focusing arrangement employed for the incident beam and the timing of the boxcar gate pulse with respect to the laser pulse. Other researchers have observed more significant effects of the laser fluence on the LII signal [12] and further research is needed in this area. However, for the conditions described in the present work, reproducible results were always obtained as long as care was taken in the alignment of the optics and achievement of a near-gaussian beam intensity profile.

The spectral response of the LII signal is shown in Fig. 6, where the LII signal is plotted as a function of the detection wavelength. The spectral scan of the LII signal has been obtained by rotating the grating in the monochromator so that the detection wavelength is varied in 10-nm increments. Measurements have been taken at the radial location where the peak soot volume fraction occurs at the 40 mm height for a probe laser beam at the 1064-nm wavelength with a beam diameter of 0.5 mm

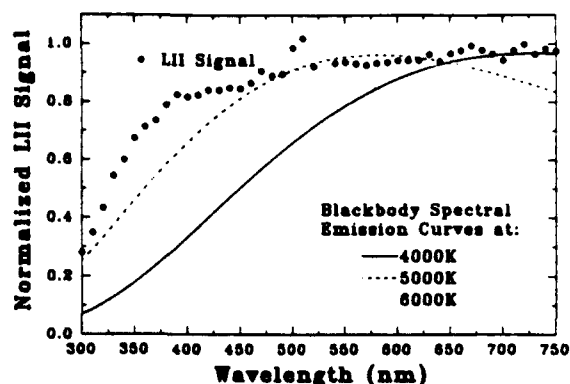


Fig. 6. Spectral response of the laser-induced incandescence where incident laser light at a wavelength of 1064 nm was used to obtain the spectrum shown.

and an energy of 1.5 mJ/pulse or laser fluence of 9.5×10^7 W/cm². For the 1064-nm wavelength laser probe beam, interference from light-scattering and PAH fluorescence is minimal in the visible wavelength range, although a fortuitous peak at 532 nm is seen due to the leakage of the 532-nm beam from the laser and corresponding light-scattering at this wavelength. It can be observed that as expected the LII signal exhibits a continuous spectra in the visible wavelength range with the signals decreasing to small levels below 300 nm. The LII spectrum also shows no distinct peaks and continues up to 750 nm at a nearly constant level. Comparison with computed blackbody radiation curves, as shown in Fig. 6, indicates that the LII spectrum in the 300–450-nm range corresponds to a soot temperature between 5000 and 6000 K, which is higher than the estimated soot vaporization temperature of ca. 4000 K. That the LII spectrum continues at a nearly constant level up to 750 nm and beyond, while the computed radiation curves begin to decline, is attributed to the fact that a large soot number density, and corresponding multiplicity of soot particle size, is present in the probe volume with different soot surface temperatures induced by the laser fluence. Hence, a more continuous and level spectral response is expected, as shown in Fig. 6 for a group of soot particles in comparison to a radiation curve computed for a single soot particle surface temperature. From Fig. 6, it can also be observed that by using 1064-nm wavelength probe laser, LII measurements can be taken at

nearly any wavelength in the visible range, except near 532 nm for our optical arrangement, due to the absence of interference from PAH fluorescence and light-scattering as noted above, and measurements taken at detection wavelengths of 400 and 700 nm have yielded identical soot volume fraction results.

The heating of the soot particles to such high temperatures may lead one to be concerned about altering the properties of the soot particles. In the present experiments we assume that the soot properties are not seriously affected by the large laser fluence before the LII measurements are made. Furthermore, since the LII signals are calibrated against independently measured soot volume fraction values, any changes introduced, as long as they are the same throughout the soot field, are compensated for in the calibration procedure. These assumptions will need to be verified in future studies, but are not anticipated to introduce errors any more significant than the present knowledge of soot properties necessarily include.

Figure 7a shows the soot volume fraction measured by LII and the vertically polarized component of the light-scattering signal (Q_{vv}), while Fig. 7b contains the data for the mean soot particle diameter and the soot number density obtained from these measurements. To obtain the results shown in Fig. 7b, the Q_{vv} and soot volume fraction measurements were analyzed in a manner similar to that described by Santoro et al. [8]. The vertically polarized light-scattering signal has been obtained for the 532-nm wavelength laser probe beam, and

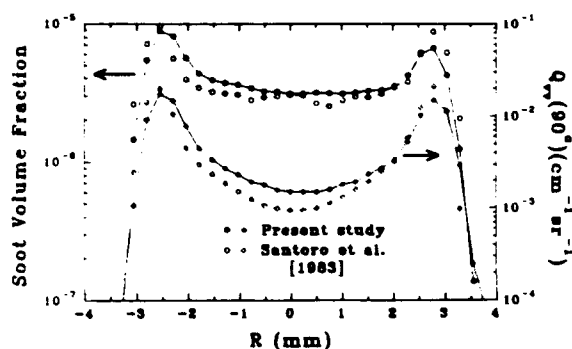


Fig. 7. (a) Radial profiles of the soot volume fraction and vertically polarized light-scattering signal, Q_{vv} , at a height, H , of 40 mm above the fuel tube exit of the burner.

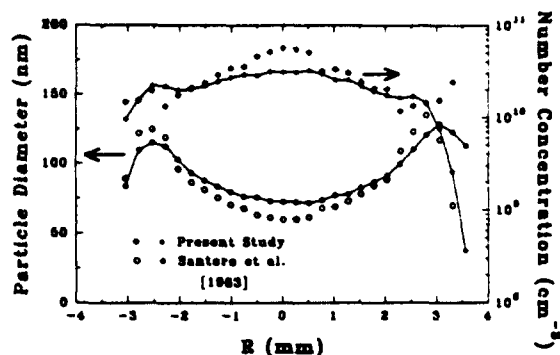


Fig. 7. (b) Radial profiles of the mean soot particle diameter, D_{63} , and soot number concentration, N , at a height, H , of 40 mm above the fuel tube exit of the burner.

the calibration for the absolute value of Q_{vv} has been obtained by matching with the known value of this signal at a single radial position using measurements by Santoro et al. [8] similar to the calibration procedure for the soot volume fraction. From the soot volume fraction and light-scattering data, which is proportional to the sixth moment of the soot particle diameter distribution, the mean soot particle diameter (D_{63}) and the soot number density (N) can be obtained as follows [8]:

$$D_{63} = \lambda^{4/3} \left(\frac{2Q_{vv}}{3\pi^3 F(\bar{m}) f_v} \right)^{1/3}, \quad (1)$$

where

$$F(\bar{m}) = \left| \frac{\bar{m}^2 - 1}{\bar{m}^2 + 2} \right|^2, \quad (2)$$

$$N = \frac{12f_v}{\pi D_{63}^3}. \quad (3)$$

Here, f_v denotes the soot volume fraction while the complex index of refraction, \bar{m} , is taken as $(1.57 - 0.56i)$ following Dalzell and Sarofim [13]. Similar to light scattering/extinction, the LII/light scattering technique yields the ratio of the sixth to third moment (D_{63}) of the particle diameter. The resultant mean soot particle diameter and the soot number density are again compared with the previous data obtained for this flame using the laser scattering/extinction method [8]. Figure 7b shows that the mean soot particle diameters are in

very good agreement, with the discrepancy being mostly limited to the central region where due to the relatively low signal levels there is the largest uncertainty in both the LII and light-scattering data. The mean soot particle diameter from LII data in the present study ranges from 75 to 130 nm, while diameters of 60–135 nm have been observed by Santoro et al. [8].

It should be noted that the particle diameters reported, in some cases, exceed the size normally considered to be appropriate for a Rayleigh theory analysis. In fact, the soot particles in this flame are aggregates composed of primary particles that do satisfy the Rayleigh theory limit [14]. Thus, strictly, D and N refer to the volume equivalent diameter and number density, respectively, of these aggregates. Particle morphology effects are not included explicitly in the current study, which would require multiple-angle light scattering measurements. However, such measurements are feasible, in principle, and represent another area where the LII technique can contribute to research related to soot particle property determination.

The soot number density profiles are similarly in reasonably good agreement with the discrepancy again occurring near the centerline. Since the number density is inversely proportional to the cube of the mean soot particle diameter, the factor of 2 difference in the soot number density near the centerline is caused by the corresponding difference in the mean soot particle diameter shown in Fig. 7b. Thus, Fig. 7b shows that the single-point or two-dimensional measurements of the LII and light scattering, which can be set up with relative ease, a complete characterization of soot particle properties may be directly obtained.

CONCLUSIONS

From the discussion above, the following conclusions concerning the LII diagnostic of soot volume fraction are made:

1. Laser-induced incandescence has been used to obtain spatially resolved measurements of soot volume fraction in laminar diffusion flames, in which comparisons with laser scattering/extinction data yield excellent

agreement for both radial profiles and integrated volume fraction. Thus, LII can be used as an instantaneous, spatially resolved diagnostic of soot volume fraction without the need for the conventional line-of-sight laser extinction method.

2. The temporal characteristics of the LII signal are observed to involve a rapid rise in intensity followed by a relatively long (ca. 600 ns) decay period subsequent to the laser pulse, while the effect of laser fluence is manifest in nonlinear and saturated response of the LII signal with the transition occurring at a laser fluence of approximately $1.2 \times 10^8 \text{ W/cm}^2$ for a laser pulse of ca. 7 ns in duration.
3. Spectral response of the LII involves a continuous spectrum in the visible wavelength range due to the blackbody nature of the emission, where the spectral response for 300–450-nm wavelength range indicates a soot surface temperature of ca. 5000 K with the spectrum continuing at a nearly level intensity up to 750-nm wavelength due to the multiplicity of the soot particle sizes in the probe volume.
4. Simultaneous measurements of LII and the vertically polarized light-scattering yield encouraging results concerning the mean soot particle diameter and number concentration; thus, significant applications exist in two-dimensional imaging and simultaneous measurements of LII and light scattering to generate a complete soot property characterization.

This material is based upon work supported by the Air Force Office of Scientific Research under Award No. F49620-92-J-0314 with Dr. Julian Tishkoff as contract manager and their support is

gratefully acknowledged. The authors would also like to thank J. A. Pinson and S. Gupta of Penn State for many useful discussions and J. E. Harrington, C. R. Shaddix, and K. C. Smyth of the National Institute of Standards and Technology for providing us with their results on the effects of laser fluence on LII signals. We would also like to acknowledge the reviewers for their suggestions regarding the light scattering analysis and the effects of aggregates on the interpretation of the results of this work.

REFERENCES

1. Melton, L. A., *Appl. Opt.* 23:2201–2208 (1984).
2. Dasch, C. J., *Appl. Opt.* 23:2209–2215 (1984).
3. Eckbreth, A. C., Bonczyk, P. A., and Verdieck, J. F., *Prog. Ener. Combust. Sci.* 5:253–322.
4. Tait, N. P., and Greenhalgh, D. A., *Proceedings of the Optical Methods and Data Processing in Heat Transfer and Fluid Flow Conference*, London, April 1992.
5. Dec, J. E., zur Loye, A. O., and Siebers, D. L., *SAE Technical Papers Series SAE-910224*, Society of Automotive Engineers, PA, 1991.
6. Dec, J., *SAE Technical Papers Series SAE-920115*, Society of Automotive Engineers, PA, 1992.
7. Eckbreth, A. C., *J. Appl. Phys.* 48:4473–4479 (1977).
8. Santoro, R. J., Semerjian, H. G., and Dobbins, R. A., *Combust. Flame* 51:203–218 (1983).
9. Santoro, R. J., Yeh, T. T., Horvath, J. J., and Semerjian, H. G., *Combust. Sci. Technol.* 53:89–115 (1987).
10. Puri, R., Moser, M., Santoro, R. J., and Smyth, K. C., *Twenty-Fourth Symposium (International) on Combustion*, The Combustion Institute, Pittsburgh, 1992, pp. 1015–1022.
11. Miller, J. H., Mallard, W. G., and Smyth, K. C., *Combust. Flame* 47:205–214 (1982).
12. Shaddix, C. R., Harrington, J. E., and Smith, K. C., personal communication.
13. Dalzell, W. H., and Sarofim, A. F., *Trans. ASME J. Heat Transf.* 91:100–104 (1969).
14. Puri, R., Richardson, T. F., Santoro, R. J., and Dobbins, R. A., *Combust. Flame* 92:320–333 (1993).

Received 15 July 1993; revised 19 January 1994